

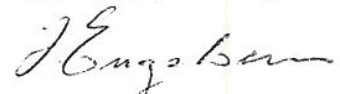
FFIU
Intern rapport U-319
Reference : 116
Date : May 1975

DECOMPOSITION OF SIGNAL ARRIVAL TIMES DUE TO
MULTIPATH CONDITIONS IN SHALLOW WATERS

by

P O Fjell

Approved
Horten, 14 May 1975



I Engelsen
Superintendent

FORSVARETS FORSKNINGSINSTITUTT
Norwegian Defence Research Establishment
P O Box 25 - N-2007 Kjeller
Norway

CONTENTS		Page
1	INTRODUCTION	3
2	THE MULTIPATH PROBLEM	3
2.1	Some basic properties of the linear multi-path problem	3
2.2	The multipath effect in inhomogeneous media	9
3	ARRIVAL TIMES EXTRACTION METHODS	11
3.1	Background	11
3.2	Decision theory	11
3.3	Correlation	14
3.4	Inverse filtering	15
3.5	Nonlinear Filtering	16
3.6	Cepstrum Technique	17
3.6.1	Background	17
3.6.2	The single echo case	19
3.6.3	The two echo case	24
3.6.4	The general m-echo case	28
3.6.5	The presence of noise	32
3.6.6	Conclusions	36
4	DATA COLLECTION	36
5	CALCULATION OF PROPAGATION PATHS	39
5.1	Sound velocity profiles	39
5.2	Calculations of ray paths	39
6	RESULTS	49
6.1	Implementation of the Cepstrum Method	49
6.2	Results from simulated data	49
6.3	Results from real data	53
6.4	Comparison with results obtained using correlation technique	59
7	CONCLUSIONS	60
	REFERENCES	61

DECOMPOSITION OF SIGNAL ARRIVAL TIMES DUE TO MULTIPATH
CONDITIONS IN SHALLOW WATERS

SUMMARY

In the present report different methods for signal decomposition of overlapping signals are discussed. No a priori knowledge of the signal is assumed. The use of non-linear filtering is found to be useful. The non-linear filtering process cepstrum is used. A theoretical treatment for different signal conditions (i e one echo, two echoes, m-echoes, noise) is given. The cepstrum method is applied to signal data from a research cruise and the results are discussed

1 INTRODUCTION

An acoustic intercept receiver uses the signals (noise, ping etc) from the target to estimate the target movements. Thus only passive estimation methods are used. The multipath structure is a possible estimator effect which may give an independent distance indication.

Multipath effects are generated when the acoustic signals are reflected from the air-water or sea-bed-water interface or when the velocity gradients changes sign. Since there may be a considerable difference in path lengths, a single sharp pulse subjected to this type of phenomena would be received as a series of pulses.

In shallow water the difference in time between the different pathlengths will be small. The received signal will therefore normally be composite signal with overlapping echoes. The problem is then to extract the different arrival times from this composite signal.

2 THE MULTIPATH PROBLEM

2.1 Some basic properties of the linear multipath problem {1}

The transmission times for well defined multipath patterns are used to calculate the distance between the source and

the receiver. It is assumed that the speed of sound is constant with depth, that is, there is a isovelocity profile. Only the configuration with the source located at the surface and the receiver located at a depth d will be considered (fig 2.1). This is an oversimplification of the physical problem and real velocity profiles will be considered later.

For the direct ray, the distance travelled between source and receiver :

$$x_0 = (r^2 + d^2)^{\frac{1}{2}} \quad (2.1.1)$$

Also for the ray reflected once from the bottom. The result is obtained by taking the mirror image of Figure 2.1 about the bottom as an axis and observing the triangle with height $z + (z-d)$ and base r . This gives

$$x_1 = (r^2 + (2z - d)^2)^{\frac{1}{2}} \quad (2.1.2)$$

By using the approach described above we have for the ray reflected twice from the bottom

$$x_3 = (r^2 + (4z - d)^2)^{\frac{1}{2}} \quad (2.1.3)$$

and generally for rays reflected at the target from the bottom (i e the last reflection is from the bottom) :

$$x_n = (r^2 + ((n+1) z - d)^2)^{\frac{1}{2}} \quad (2.1.4)$$

for $n = 1, 3, 5 \dots$

where n is the total number of reflections from surface and bottom.

Now for the ray reflected at the target from the surface (i e the last reflection is from the surface) :

$$x_2 = (r^2 + (2z + d)^2)^{\frac{1}{2}} \quad (2.1.5)$$

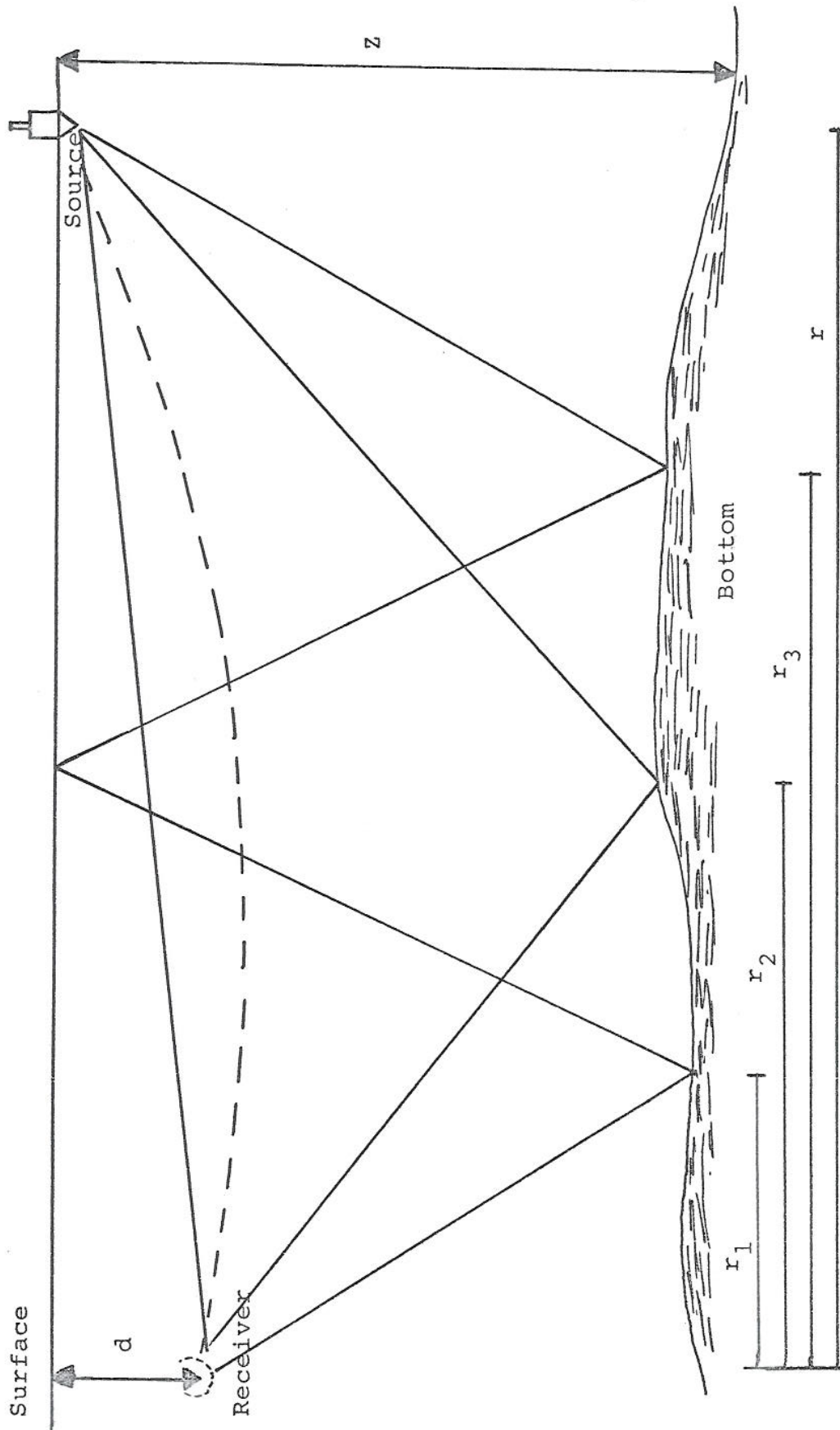


Figure 2.1 The multipath structure

and

$$x_4 = (r^2 + (4z + d)^2)^{\frac{1}{2}} \quad (2.1.6)$$

so that

$$x_n = (r^2 + (nz + d)^2)^{\frac{1}{2}} \quad (2.1.7)$$

$$n = 0, 2, 4 \dots$$

where n is the total number of reflections from surface and bottom.

The transmission time differences for this linear velocity case is

$$\Delta T = \frac{\Delta x}{c}$$

where Δx is the difference in path length and c is the velocity of sound assumed to be constant. From (2.1.4) and (2.1.7) we get :

$$\begin{aligned} \Delta x &= x_m - x_n \\ &= (r^2 + ((m+1)z-d)^2)^{\frac{1}{2}} - (r^2 + (nz+d)^2)^{\frac{1}{2}} \\ &= (r^2 + A^2)^{\frac{1}{2}} - (r^2 + B^2)^{\frac{1}{2}} \end{aligned}$$

where

$$A = ((m+1)z-d)^2$$

$$B = (nz + d)^2$$

or

$$(\Delta x)^2 = 2r^2 + (A^2 + B^2) - 2(r^2 + A^2)^{\frac{1}{2}} (r^2 + B^2)^{\frac{1}{2}}$$

or

$$r^2 + \frac{1}{2}(A^2+B^2-(\Delta x)^2) = (r^2+A^2)^{\frac{1}{2}}(r^2+B^2)^{\frac{1}{2}}$$
$$r^2+C^2 = (r^2+A^2)^{\frac{1}{2}}(r^2+B^2)^{\frac{1}{2}}$$

where

$$C^2 = \frac{1}{2}(A^2+B^2-(\Delta x)^2)$$

or

$$(r^2+C^2)^2 = (r^2+A^2)(r^2+B^2)$$

$$r^4+2r^2C^2+C^4 = r^4+r^2(A^2+B^2)+A^2B^2$$

$$r^2(A^2+B^2-2C^2) = C^4-A^2B^2$$

or

$$r^2 = \frac{C^4 - A^2B^2}{A^2+B^2-2C^2}$$

or

$$r = \pm \left(\frac{C^4 - A^2B^2}{A^2+B^2-2C^2} \right)^{\frac{1}{2}} \quad (2.1.8)$$

Now A, B and C contains the depth z, which we know, the depth d of the receiver which is known and the time difference ΔT between different transmission paths which we assume can be measured. Thus we can find the distance r to the target.

This is of course an idealised situation. The velocity profile is not constant and so the simple geometrical model given here is not valid. Some quite useful conclusions can, however, be drawn. If in (2.1.8) we substitute the expressions for A, B and C, the order of magnitude of ΔT for different r, d, n and z can be calculated. Fig 2.2 shows this for $\bar{d} = 200$ m, $z = 400$ m and $n = 0, 1, 2$. It is seen that as the distance to the target increases the

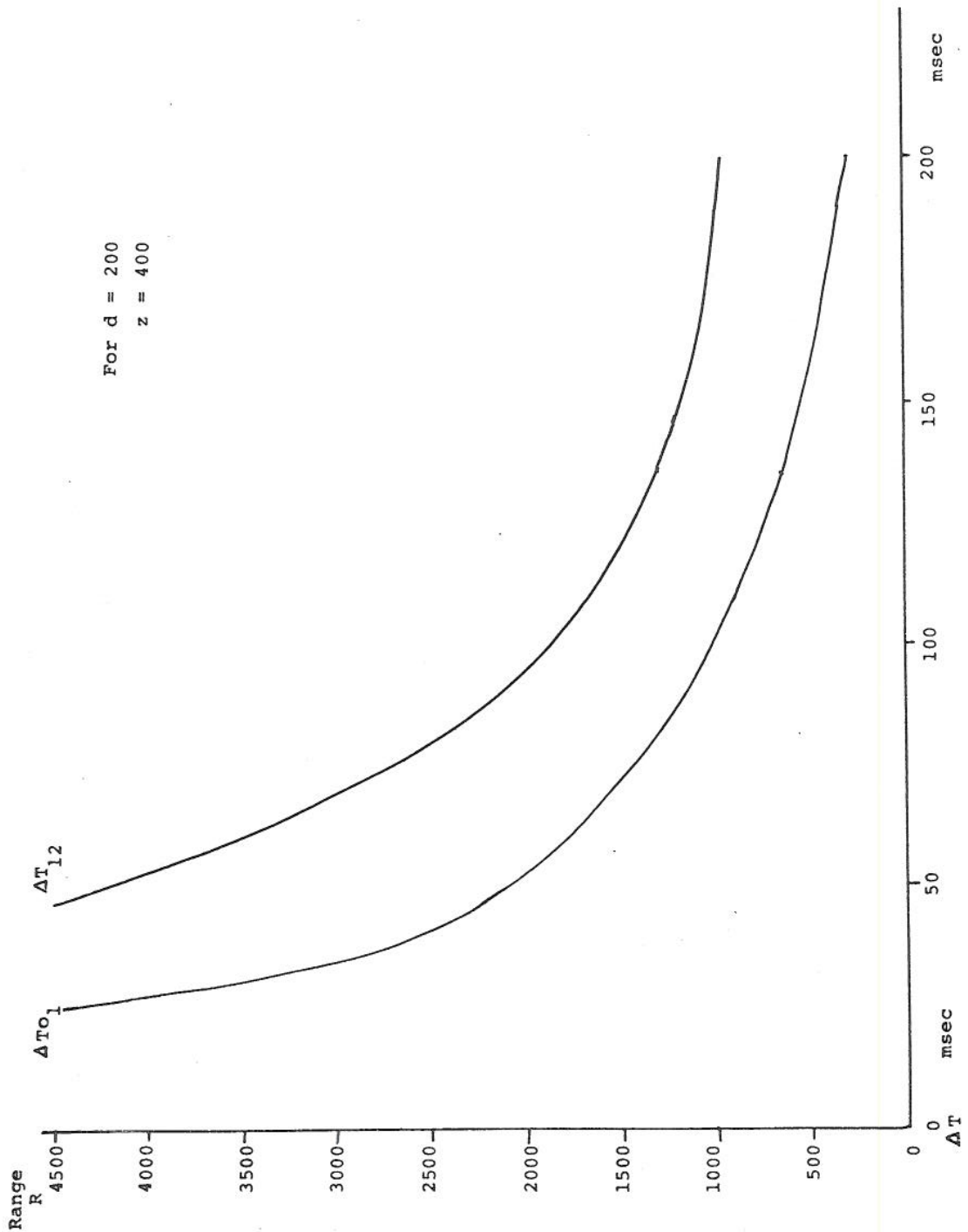


Figure 2.2 Time difference between the first two arrival times

time difference will decrease in a hypobolic way. Thus a finer resolution for a composite signal from a great distance than from a small one is needed and hence adding to the problem since the signal to noise ratios will decrease with distance.

2.2 The multipath effect in inhomogeneous media

A variation of the sound velocity in water will cause bending of the signal path. Fig 2.3.

Let a ray at bearing angle ϕ_0 link the target to the receiver in an ocean with an index of refraction $n(h)$. It is straight forward to determine in an elementary way the coordinates (h,R) of the ray. {34}, {35}. We obtain :

$$R_T = \cos \phi_0 \int_0^h n^2 (n^2 - \cos^2 \phi_0)^{-\frac{1}{2}} dh \quad (2.2.1)$$

The travel time t_0 along a ray determined by the bearing line ϕ_0 is

$$t_0 = \frac{1}{c_0} \int_0^h n^2 (n^2 - \cos^2 \phi_0)^{-\frac{1}{2}} dh \quad (2.2.2)$$

where c_0 is the average velocity at the receiver.

A computation of the direct ray transmission time will give us an estimation of the distance to the target ship. We see, however, that the computational methods will get fairly involved for complex velocity profiles.

The scattering of sound waves at the sea surface has been the subject of considerable studies. To date, a consistent theory that explains the various phenomena observed is lacking. The scattering effect will distort the reflected signals in some way. This creates a problem since one no longer have echoes which are replicas of the original signal at the receiver, but echoes distorted to some extent in an unpredictable way.

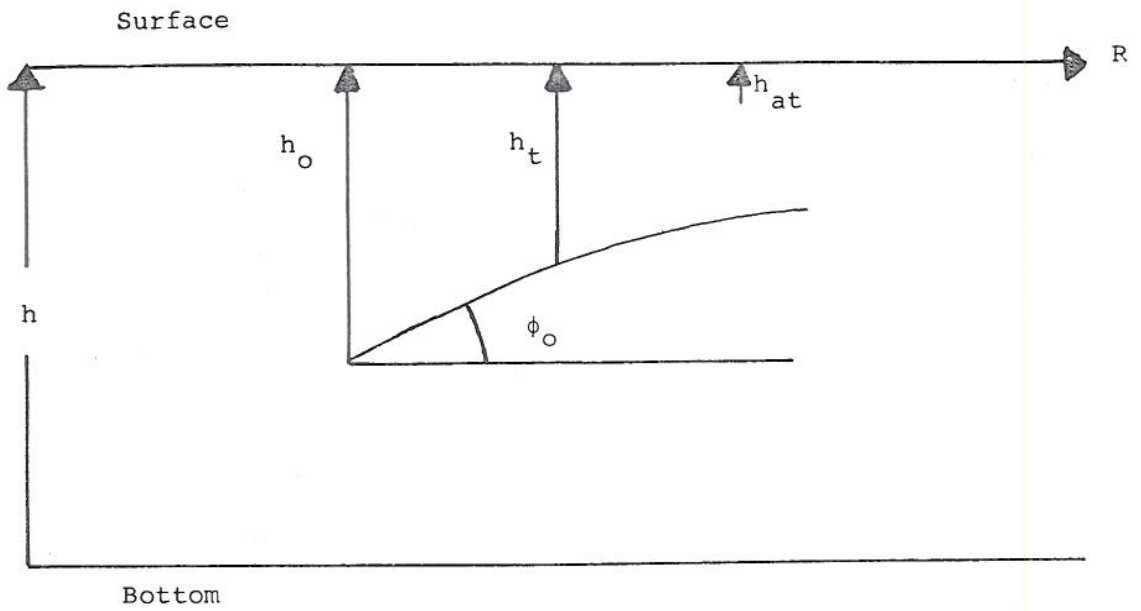


Figure 2.3 The bending of the signal

3 ARRIVAL TIMES EXTRACTION METHODS

3.1 Background

The problem can be formulated in the following way. Given a signal which is a finite summation of basic wavelets immersed in a noisy environment with stochastic parameters, estimate the arrival-times (or epochs). This report presents an approach and solution to this problem with certain limitations. The general problem of the decomposition of composite stochastic processes is not solved, nor is the one where the overlapping wavelets are of different form. In this report it is, as stated above, assumed that the wavelets may be multiple, but must be identical in waveshape, although this waveshape is unknown.

3.2 Decision theory

In {2} an algorithm is discussed which decomposes a noisy composite signal of identical, but unknown multiple wavelet, overlapping in time. The decomposition determines the number of wavelets present, their epochs, amplitudes and an estimate of the basic wavelet shape.

The algorithm is an adaptive decomposition filter which is a combination of three separate filters. One is an adaptive cross-correlation filter which resolves the composite signal from noise by an iteration procedure. This is followed by a wavelet extraction filter which ferrets out the basic wavelet form, and last there appears an inverse filter which achieves decomposition of the composite signal in the time domain.

Decision theory can be applied when noise is present to estimate the arrival times. This is a straightforward approach if the signal waveshape is known {3}. In practice, however, this requirement will make this method unsuitable.

A block diagram of the overall adaptive decomposition filter is given in fig 3.1 and fig 3.2 gives a flow-chart of the algorithm used. Some of the different terms used

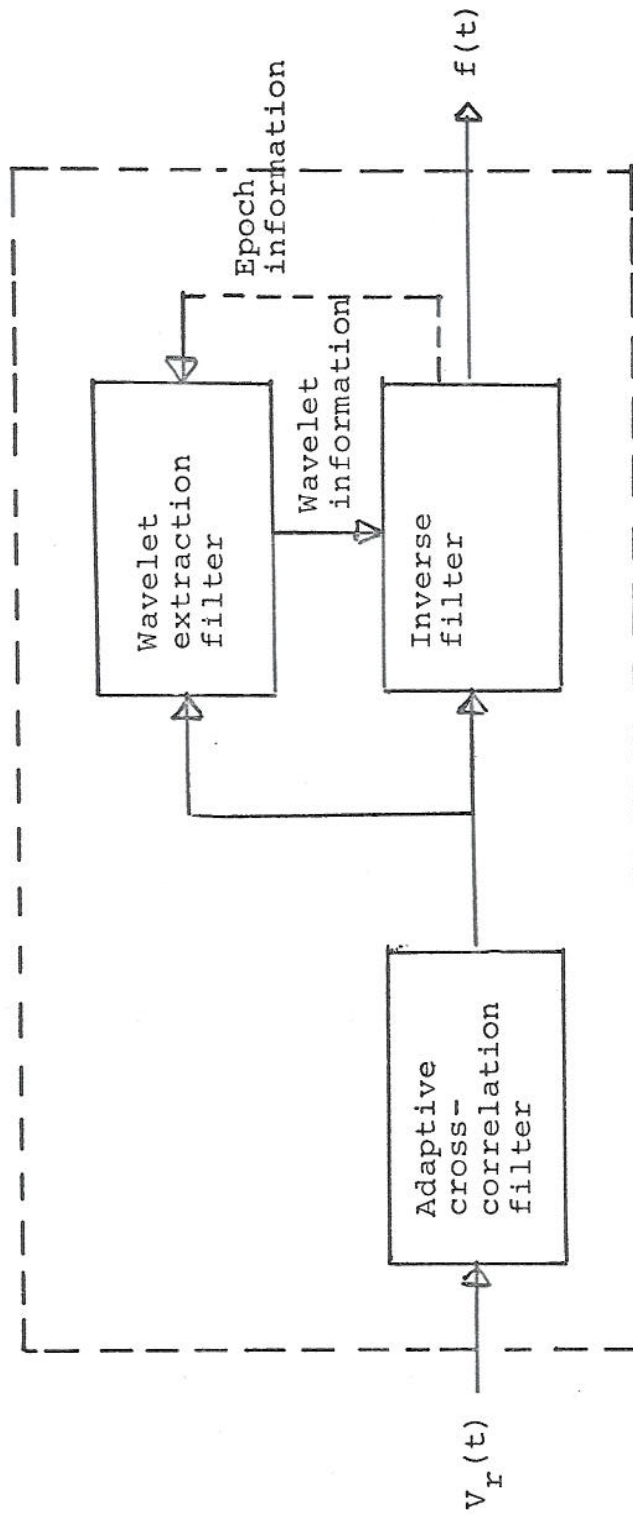


Figure 3.1 Block diagram of overall adaptive decomposition filter

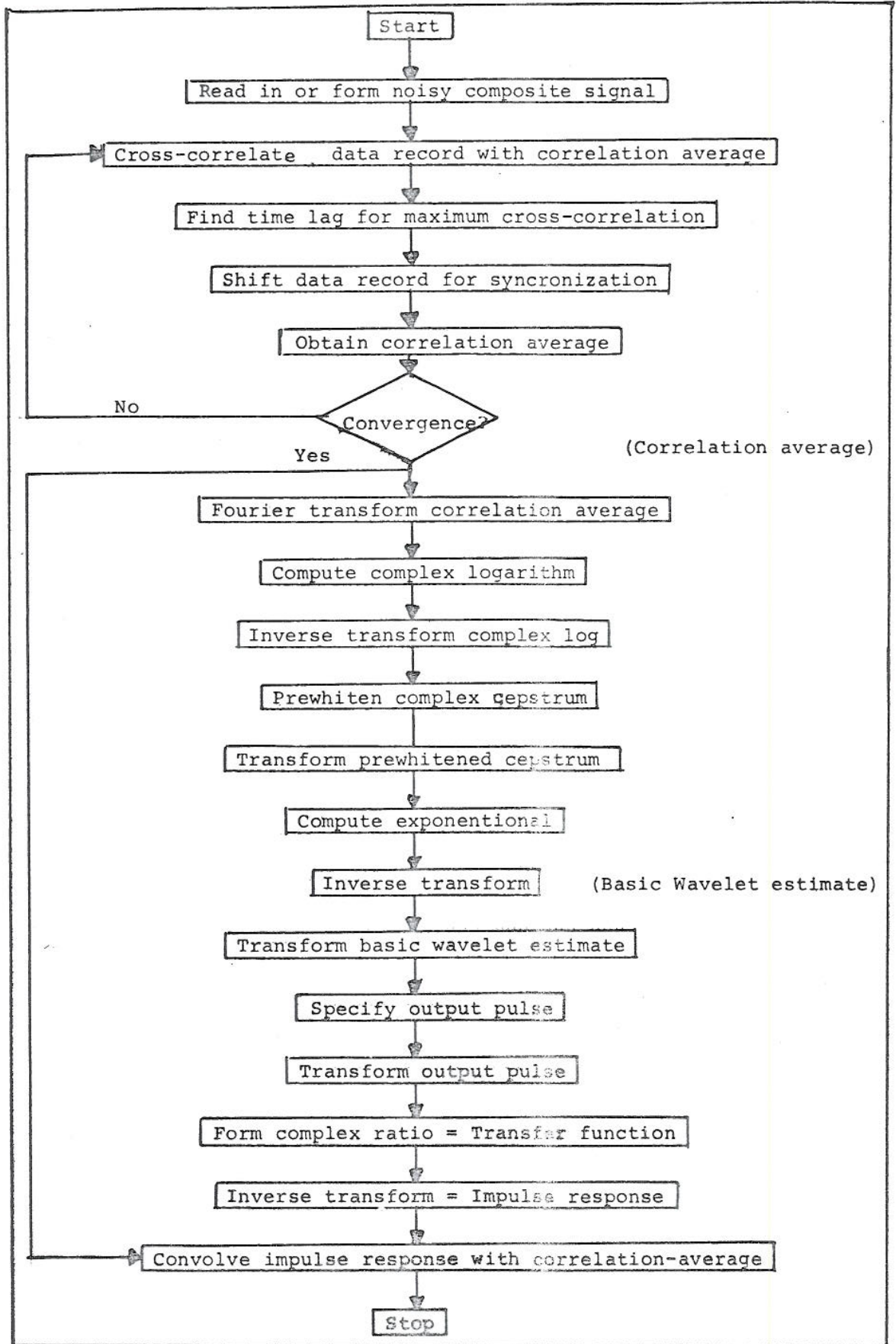


Figure 3.2 Algorithm flow-chart

is defined in section 3.6 below or ref {2}.

The implementation of this algorithm on a computer will necessarily be a fairly big system and calculation time will be fairly long (> 5 secs).

One weakness with {2} is that only simulated data are used. It is of some interest to note that most of the papers available on signal decomposition problems deals with simulated data.

3.3 Correlation

The use of auto - or cross-correlation methods are well known and will not be elaborated in this report.

The use of correlation techniques are discussed in {29}, {30} and the results are summarized below.

The auto-correlation of the received signal may be obtained through an inverse FFT of the power spectrum. The delay time τ , obtained from the time difference between the two highest peaks, is associated with the relative positions of target and receiver. For a non-periodic signal, the resolution of the peaks is possible when the delay time τ is at least greater than the correlation time of the signal. The correlation length has an inverse relationship to the bandwidth of the signal.

In some situations such as long range or shallow water the correlation time is greater than the delay time and the autocorrelation will lack the resolvability needed.

With a sinusoidal present the auto-correlation does not die out, as τ increases. This causes a failure of the straight auto-correlation scheme when the auto-correlation of the interfering sinusoid can smear over the wideband contribution of the echo. It is however possible

to filter out these sinusoids by smoothing the peaks to a local level in the power spectrum before computing the auto-correlation function. The use of the cepstrum is found to exercise much greater discrimination against unfiltered sinusoids than autocorrelation, but it shows a greater sensitivity to differences in distortion between the paths of the channel.

For a sinusoidal signal (as used in the experiments in this report) the auto-correlation technique is thus unsuitable.

The use of cross-correlation is not applicable since no a priori knowledge of the signal is assumed.

3.4 Inverse filtering

In the application of inverse filtering, the signal is transformed by a linear time-invariant system, whose Fourier transform is the reciprocal of the transform of the signal components to be removed. In {3} it is pointed out that this method has a serious limitation. The signal must be known and the signal-to-noise ratio (SNR) must be quite large. Investigations that attempted to employ a Wiener filter to improve the estimates of decomposition proved to be of little value {4}. For high SNR this filter is unnecessary, for low-input SNR the system acts like a matched filter that is unsuitable for decomposition unless one wishes to decompose signals where time of occurrence between signals is approximately twice the length of the signal duration. (One may note here that a matched filter is not suited to general signal resolution of overlapping signals).

In {5} it is stated that it is difficult to achieve composite signal decomposition via inverse filtering in the presence of noise. Arbitrarily large SNR and good resolution cannot be simultaneously achieved at the output of an inverse filter because of conflicting require-

ments. If the output pulse is made narrow to achieve good resolution, then this, in term, means that the filter bandwidth is large, which, in term, implies that the output noise level is increased. A compromise must be made which selects a pulsewidth to achieve decomposition in the presence of noise.

In {6}, {7} and {8} some further points of inverse filtering is discussed and in {9} the use of inverse filtering is used in speech analysis.

Since this method assumes a knowledge of the signal shape it is unsuitable as decomposition method for unknown wavelets.

3.5 Nonlinear Filtering

There has been an increased interest in nonlinear filtering over recent years. The literature on nonlinear filtering tends to fall into two areas {10}. In the first area, nonlinear filters are derived mathematically from various optimum or suboptimum solutions of nonlinear estimation problems. The other area involves a deterministic approach and is typified by the class of homomorphic filters examined by {11}.

The class of homomorphic filters considered by {10} are characterized by having the property that if $s_1(\tau)$ and $s_2(\tau)$ are two signals combined by some rule denoted by \circ , then the filter has the property :

$$\phi(s_1(t) \circ s_2(t)) = \phi(s_1(t)) \circ \phi(s_2(t)) \quad (3.5.1)$$

where ϕ represents the filter transformation.

This is synonymous with the additive property for the special case of linear systems where \circ corresponds to addition. The generalization of the homogeneous property is stated as

$$\phi(c : s(t)) = c : \phi(s(t)) \quad (3.5.2)$$

where c is a scalar and the colon denotes the product of the input with the scalar.

A filter which satisfies both (3.5.1) and (3.5.2) is called a homomorphic filter. A homomorphic filter can be realized by a number of systems in cascade as shown in figure 3.3.

The first system A_0 has the property that

$$A_0(s_1(t) \circ s_2(t)) = A_0(s_1(t)) + A_0(s_2(t)) \quad (3.5.3)$$

and

$$A_0(c : s(t)) = c : A_0(s(t)) \quad (3.5.4)$$

The system L is a linear filter and A_0^{-1} is the inverse of A_0 , i e

$$A_0^{-1}\{A_0(s(t))\} = s(t) \quad (3.5.5)$$

The application of this principle for convolved signals usually involves a process called cepstrum analysis and has been elaborated below. The cepstrum analysis method will be used in our analysis of composite signal decomposition.

Other applications of nonlinear filtering can be found in {10}, {12}, {13}, {14} and {15}.

3.6 Cepstrum Technique

3.6.1 Background

There are several different definitions of the Cepstrum method. We use the following definition :

Definition : The power cepstrum of a function is the power spectrum of the logarithm of the power spectrum of that function.

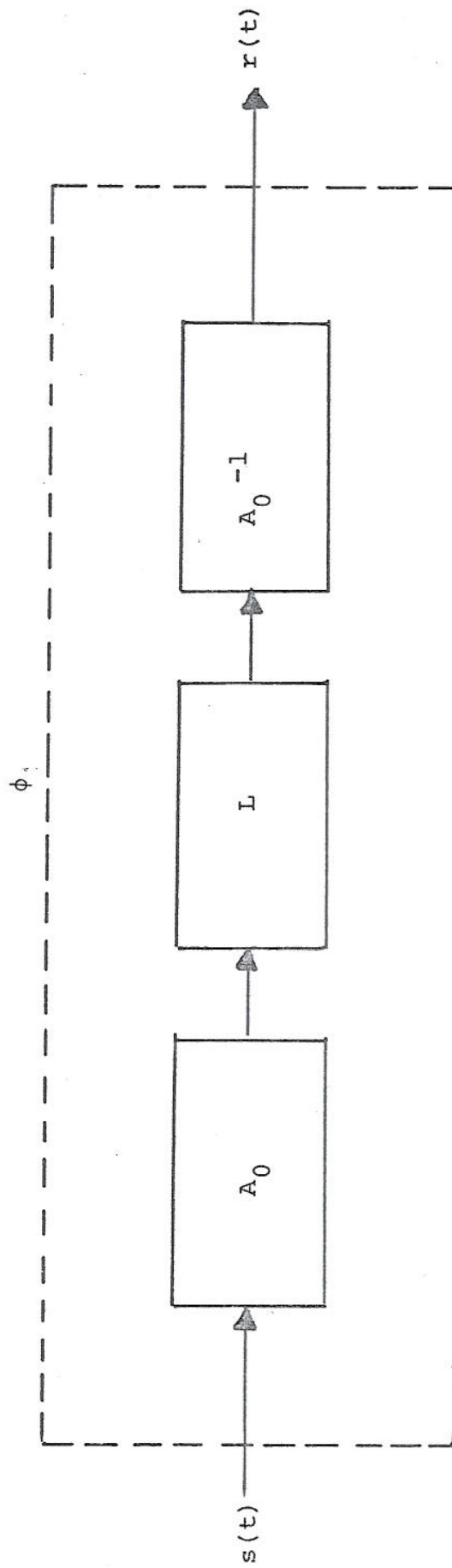


Figure 3.3 Realization of homomorphic filter

The cepstrum technique has become fairly popular as a method to decompose composite signals. The technique was introduced by {19} and it found a wide use in speech synthesis {20}, {21} , {22}, {23} and {24}. For other applications the use of the cepstrum was also popular {3}, {18}, {17}, {16}, {29} and {30}.

3.6.2 The single echo case

(By echo we mean a signal which due to the multipath effect travel a different way than the first signal arrival).

To explain the power cepstrum analysis a simple example will be considered. We have the original signal $s(t)$ and one echo. It follows :

$$x(t) = s(t) + a_0 s(t-t_0) \quad (3.6.2.1)$$

where $x(t)$ is the composite signal

$s(t)$ is the original signal

a_0 is the echo amplitude

t_0 is the time difference with respect to the original signal

The power spectrum can then be written

$$G_x(\omega) = G_s(\omega) (1 + a_0^2 + 2 a_0 \cos \omega t_0) \quad (3.6.2.2)$$

since

$$\begin{aligned} X(j\omega) &= \int_{-\infty}^{+\infty} x(t) e^{-j\omega t} dt \\ &= \int_{-\infty}^{+\infty} (s(t) + a_0 s(t-t_0)) e^{-j\omega t} dt \\ &= S(j\omega) (1+a_0 e^{-j\omega t_0}) \end{aligned} \quad (3.6.2.3)$$

and

$$\begin{aligned}
 G_x(\omega) &= \lim_{T \rightarrow \infty} \frac{2}{T} \overline{|X(j\omega)|^2} \\
 &= \lim_{T \rightarrow \infty} \frac{2}{T} \overline{|S(j\omega)|^2 |1 + a_0 e^{-j\omega t_0}|^2} \\
 &= G_s(\omega) (1 + a_0^2 + 2a_0 \cos \omega t_0) \quad (3.6.2.4)
 \end{aligned}$$

Using the definition of the power cepstrum we get :

$$\begin{aligned}
 \ln G_x(\omega) &= \ln (G_s(\omega) (1 + a_0^2 + 2a_0 \cos \omega t_0)) \\
 &= \ln (G_s(\omega)) + \ln (1 + a_0^2 + 2a_0 \cos \omega t_0) \quad (3.6.2.5)
 \end{aligned}$$

(3.6.2.5) shows that $\ln G_x(\omega)$ has a cosine like ripple, with period and amplitude connected with the echo parameters a_0 and t_0 . This ripple is difficult to directly detect in the log power spectrum and we are forced to use traditionally methods in detecting a periodic function in noise. We can therefore apply the power spectrum analysis again and we have what is known as the power cepstrum.

The second part of (3.6.2.5) can now be expanded in a suitable converging infinite serie.

This leads to some interesting properties. We have that :

$$\ln (1+x) = x - \frac{x^2}{2} + \frac{x^3}{3} \dots \quad |x| \leq 1 \quad (3.6.2.6)$$

This will limit the amplitude a_0 (the echo amplitude), and also t_0 the echo epoch. Stringent mathematical form will give :

$$-0.41 \leq a_0 \leq 0.41. \quad (\text{for } a_0 < 1) \quad (3.6.2.7)$$

$$a_0 > 2.4 \quad (\text{for } a_0 > 1)$$

In practice these limits will be disregarded as $\cos \omega t_0$ seldom is 1, thus a_0 can vary between greater limits.

These constraints are given in {3} and {25}. In {16} it is pointed out that these conditions preclude the cepstrum of the application for many interesting problems. Such is the case when the index of refraction changes abruptly at the boundary or the reflecting layer is nondissipative. For operations near a calm ocean surface, the reflection coefficient is close to -1, and a_0 falls outside the region $|a_0| < 0.41$. Then for practical frequency $f = n / t_0$, $n = 0, \pm 1, \dots$, the cepstrum is supposed to fail. The same conclusion follows when the source is moving out of the shadow region into the illuminated region. The value of a_0 falls outside the region $2.4 < |a_0| < \infty$. Further one can note that $|a| > 0.41$ is highly desirable for facilitating the extraction of time delay in a very noisy environment such as the ocean.

Since in many instances the bounds set on a_0 are not obeyed, it seems worthwhile to point out that these bounds appear unnecessarily stringent. The power spectrum is given in (3.6.2.2).

$$G_x(\omega) = G_s(\omega) (1 + a_0^2 + 2a_0 \cos \omega t_0)$$

If we factorize (3.6.2.2) by taking the factor $(1 + a_0^2)$ and then take the log of (3.6.2.2) we have

$$\ln G_x(\omega) = \ln(1 + a_0^2) G_s(\omega) + \ln(1 + \alpha \cos \omega t_0) \quad (3.6.2.8)$$

$$\text{where } \alpha = 2a_0 / (1 + a_0^2)$$

α has a maximum and a minimum at ± 1 for $0 < |a_0| \leq \infty$. Then $\alpha \cos \omega t_0$ prevents us from expanding $\ln(1 + \alpha \cos \omega t_0)$ in an infinite series only for the point values $\alpha = \pm 1$ and $\cos \omega t_0 = \pm 1$.

Otherwise we have :

$$\ln(1 + \alpha \cos \omega t_0) = \sum_{k=1}^{\infty} (-1)^{k+1} (\alpha \cos \omega t_0)^k / k \quad (3.6.2.9)$$

Expressing the $(\cos \omega k_0)^k$ terms in terms of $\cos k \omega t_0$ and taking the Fourier transform of (3.6.2.9), we find that the cepstrum would display a dominant peak at the delay time t_0 regardless of the size of a_0 . Thus the constraints given initially depends except for $\alpha = \pm 1$, $\cos \omega t_0 = \pm 1$, only on the mathematical method and not on the physics of the problem.

From (3.6.2.3) and (3.6.2.6) we get :

$$\ln G_x(\omega) = \ln G_s(\omega) + \ln (1+x) \quad (3.6.2.10)$$

$$\text{where } x = a_0^2 + 2a_0 \cos \omega t_0$$

so that

$$\begin{aligned} \ln G_x(\omega) &= \ln G_s(\omega) + x - \frac{x^2}{2} + \frac{x^3}{3} \dots \\ &= \ln G_s(\omega) + a_0(a_0 + 2 \cos \omega t_0) \\ &\quad - \frac{1}{2} a_0^2 (a_0^2 + 4a_0 \cos \omega t_0 + 4 \cos^2 \omega t_0) \\ &\quad + \frac{1}{3} a_0^3 (a_0^3 + 6a_0^2 \cos \omega t_0 + 12a_0 \cos^2 \omega t_0 \\ &\quad + 8 \cos^3 \omega t_0) + \dots \end{aligned} \quad (3.6.2.11)$$

or

$$\begin{aligned} \ln G_x(\omega) &= \ln G_s(\omega) + a_0^i + a_0^{ii} \cos \omega t_0 \\ &\quad + a_0^{iii} \cos^2 \omega t_0 + a_0^{iv} \cos^3 \omega t_0 + \dots \end{aligned} \quad (3.6.2.12)$$

where

$$a_0^i = a_0^2 \left(1 - \frac{1}{2} a_0^2 + \frac{1}{3} a_0^4\right)$$

$$a_0^{ii} = 2a_0(1 - a_0^2 + a_0^4)$$

$$a_o^{iii} = -2a_o^2(1-2a_o^2)$$

$$a_o^{iv} = 8/3 a_o^3$$

The power cepstrum is then deduced from :

$$Y(\tau) = \int_{-\infty}^{+\infty} (\ln G_s(\omega) + a_o^i + a_o^{ii} \cos \omega t_o + a_o^{iii} \cos^2 \omega t_o + a_o^{iv} \cos^3 \omega t_o + \dots) e^{-j\omega t} dt \quad (3.6.2.13)$$

$$= A\delta(t) + B(\delta(t-t_o) + \delta(t+t_o))$$

$$+ C(\frac{1}{2}\delta(t+2t_o) + \delta(t) + \frac{1}{2}\delta(t-2t_o)) + \dots \quad (3.6.2.14)$$

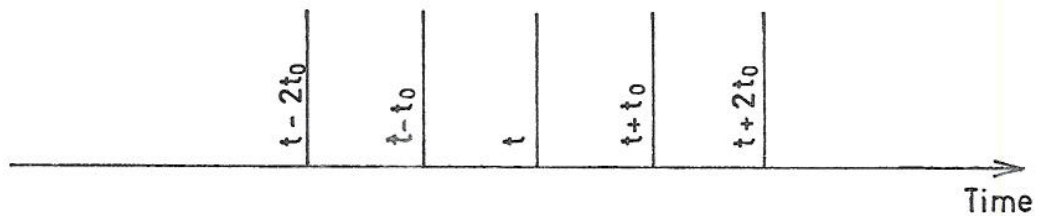


Figure 3.4 The power cepstrum of a signal with one identical echo at time t_o . The amplitude variation is not considered. Other delta functions will be present at the extremes of the time base

where $A = 2\pi(\ln G_s(\omega) + a_0^i)$

$$B = \pi a_0^{ii}$$

$$C = \pi a_0^{iii}$$

$\delta(t)$ = Dirac delta function

We therefore notice from the power cepstrum (3.6.2.14) that we have delta functions at quefrequency t_0 (an anagram of the word frequency, see {19}) and multiple t_0 . The amplitude depends on both the echo amplitude a_0 and the epoch t_0 .

When the echo amplitude $a_0 > 1$ we must write :

$$\begin{aligned} \ln G_s(\omega) &= \ln G_s(\omega) + \ln(1 + a_0^2 + 2a_0 \cos \omega t_0) \\ &= \ln G_s(\omega) + \ln(a_0^2 (1 + 1/a_0^2 + 2/a_0 \cos \omega t_0)) \\ &= \ln(a_0^2 G_s(\omega)) + \ln(1 + 1/a_0^2 + 2/a_0 \cos \omega t_0) \quad (3.6.2.15) \end{aligned}$$

It is now possible to use the same mathematical technique as above with the mathematical constraints $2.4 \leq a_0 \leq \infty$. The remarks above with respect to $|a_0|$ value is still valid, and we see that we obtain delta functions at the echo-epoch t_0 and multiple t_0 in this new power-cepstrum.

3.6.3 The two echo case

In a multipath situation in shallow water several echoes will exist. If we start to extend our mathematical analysis in the multiple echo case by first considering two echoes, we have :

$$x(t) = s(t) + a_0 s(t-t_0) + a_1 s(t-t_1) \quad (3.6.3.1)$$

where

$x(t)$ is the composite signal

$s(t)$ is the original signal

a_0 is the amplitude of the first echo

t_0 is the delay time of the first echo

a_1 is the amplitude of the second echo

t_1 is the delay time of the second echo

and hence :

$$X(j\omega) = S(\omega) (1 + a_0 \exp(-j\omega t_0) + a_1 \exp(-j\omega t_1)) \quad (3.6.3.2)$$

and the power spectrum :

$$\begin{aligned} G_x(\omega) &= \lim_{T \rightarrow \infty} \frac{2}{T} \overline{|X(j\omega)|^2} \\ &= G_s(\omega) ((1 + a_0 \cos \omega t_0 + a_1 \cos \omega t_1)^2 \\ &\quad + (a_0 \sin \omega t_0 + a_1 \sin \omega t_1)^2) \\ &= G_s(\omega) (1 + a_0^2 + a_1^2 + 2a_0 \cos \omega t_0 \\ &\quad + 2a_1 \cos \omega t_1 + 2a_0 a_1 \cos \omega (t_0 - t_1)) \end{aligned} \quad (3.6.3.3)$$

or taking the logarithm and expanding in power series :

$$\ln G_x(\omega) = \ln G_s(\omega) + x - \frac{x^2}{2} + \frac{x^3}{3} \dots \quad |x| < 1 \quad (3.6.3.4)$$

where $x = a_0^2 + a_1^2 + 2a_0 \cos \omega t_0 + 2a_1 \cos \omega t_1$

$$+ 2a_0 a_1 \cos \omega (t_0 - t_1)$$

After some manipulation we get :

$$\begin{aligned} \ln G_x(\omega) = \ln G_s(\omega) & \\ & + A + B \cos \omega t_0 + C \cos \omega t_1 \\ & + D \cos \omega(t_1 - t_0) + E \cos \omega(t_1 + t_0) \\ & + F \cos 2 \omega t_0 + G \cos 2 \omega t_1 \\ & + H \cos 2 \omega(t_1 - t_0) + I \cos \omega(t_1 - 2t_0) \\ & + J \cos \omega(2t_1 - t_0) + \dots \end{aligned} \tag{3.6.3.5}$$

where

$$A = -a_0^4/2 - a_1^4/2 - 2a_0^2 a_1^2$$

$$B = 2a_0 - 2a_0^3 - 4a_0 a_1^2$$

$$C = 2a_1 - 2a_1^3 - 4a_0^2 a_1$$

$$D = -2a_0 a_1^3 - 2a_0^3 a_1$$

$$E = -2a_0 a_1$$

$$F = -a_0^2$$

$$G = -a_1^2$$

$$H = -a_0^2 a_1^2$$

$$I = -2a_0^2 a_1$$

$$J = -2a_0 a_1^2$$

The power cepstrum can then be deduced from :

$$\begin{aligned}
 Z(\omega) = & \int_{-\infty}^{-\infty} (\ln G_S(\omega) + A + B \cos \omega t_0 + C \cos \omega t_1 \\
 & + D \cos \omega(t_1 - t_0) + E \cos \omega(t_1 + t_0) \\
 & + F \cos 2\omega t_0 + G \cos 2\omega t_1 + \\
 & H \cos 2\omega(t_1 - t_0) + I \cos \omega(t_1 - 2t_0) \\
 & + J \cos \omega(2t_1 - t_0) + \dots) e^{-j\omega t} dt \quad (3.6.3.6)
 \end{aligned}$$

$$\begin{aligned}
 = & a\delta(t) + b(\delta(t-t_0) + \delta(t+t_0)) \\
 & + c(\delta(t-t_1) + \delta(t+t_1)) + d(\delta(t-t_1+t_0) \\
 & + \delta(t+t_1-t_0)) + e(\delta(t-t_1-t_0) + \\
 & \delta(t+t_1+t_0)) + f(\delta(t-2t_0) + \delta(t+2t_0)) \\
 & + g(\delta(t-2t_1) + \delta(t+2t_1)) + h(\delta(t-2t_1+2t_0) \\
 & + \delta(t+2t_1-2t_0)) + i(\delta(t-t_1+2t_0) + \delta(t+t_1-2t_0)) \\
 & + j(\delta(t-2t_1+t_0) + \delta(t+2t_1-t_0)) + \dots \quad (3.6.3.7)
 \end{aligned}$$

where

$$\begin{aligned}
 a & = 2\pi(\ln G_S(\omega) + A) \\
 b & = \pi B \\
 c & = \pi C \\
 \cdot & \quad \cdot \\
 \cdot & \quad \cdot \\
 \cdot & \quad \cdot \\
 j & = \pi J
 \end{aligned}$$

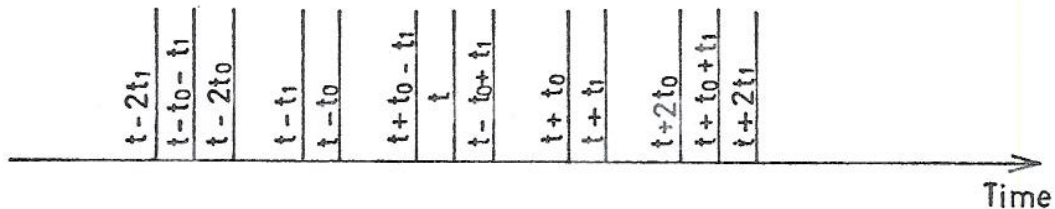


Figure 3.5 The power cepstrum of a signal with two identical echoes at t_0 and t_1 . The amplitude variation is not considered. Other delta functions will be present at the extremes of the time base. Note the increase in the number of delta functions from the single echo case (figure 5.3.4)

There are several quite distinctive features in this expression.

- (a) We get delta functions at both t_0 and t_1
- (b) We also get delta functions at many symmetrical axis about t_0 and t_1
- (c) The amplitudes of the delta function speaks are dependent upon both reflection coefficients a_0 and a_1 and both the time difference between the two echoes t_0 and t_1 and between the original signal and the first echo.

If the amplitude(s) $|a_0|$, $|a_1| > 1$ we must use the appropriate procedure discussed above, and factorize out a_0 and/or a_1 from the expression.

3.6.4 The general m-echo case

As noticed above the multipath case will consist of several echoes dependent upon the velocity profile of

sound in water. For a general expression for m echoes ($m= 0, 1, \dots n$) with arrival times $t_0 \dots t_n$ and amplitudes $a_0 \dots a_n$ ($|a_n| < 1$) we have :

$$x(t) = s(t) + a_0 s(t-t_0) + a_1 s(t-t_1) + a_2 s(t-t_2) + \dots + a_n s(t-t_n) \quad (3.6.4.1)$$

Therefore

$$X(j\omega) = S(\omega) (1 + a_0 e^{-j\omega t_0} + a_1 e^{-j\omega t_1} + a_2 e^{-j\omega t_2} + \dots + a_n e^{-j\omega t_n}) \quad (3.6.4.2)$$

$$= S(\omega) \left(1 + \sum_{k=0}^{k=n} a_k e^{-j\omega t_k} \right)$$

or

$$G_x(\omega) = G_s(\omega) \left\{ \left(1 + \sum_{k=0}^{k=n} a_k \cos \omega t_k \right)^2 + \left(\sum_{k=0}^{k=n} a_k \sin \omega t_k \right)^2 \right\}$$

$$= G_s(\omega) \left(1 + 2 \sum_{k=0}^{k=n} a_k \cos \omega t_k + \sum_{k=0}^{k=n} \sum_{i=0}^{i=n} a_k a_i \cos \omega (t_k - t_i) \right) \quad (3.6.4.3)$$

and hence :

$$\ln G_x(\omega) = \ln G_s(\omega) + \ln \left(1 + 2 \sum_{k=0}^{k=n} a_k \cos \omega t_k + \sum_{k=0}^{k=n} \sum_{i=0}^{i=n} a_k a_i \cos \omega (t_k - t_i) \right)$$

$$= \ln G_s(\omega) + x - x^2/2 + x^3/3 - \dots \quad (3.6.4.4)$$

where

$$x = 2 \sum_{k=0}^{k=n} a_k \cos \omega t_k + \sum_{k=0}^{k=n} \sum_{i=0}^{i=n} a_k a_i \cos \omega(t_k - t_i)$$

Inserting for x and carrying out some manipulation gives (neglecting the x^3 term) :

$$\ln G_X(\omega) = \ln G_S(\omega) + 2 \sum_{k=0}^{k=n} a_k \cos \omega t_k$$

$$- \sum_{k=0}^{k=n} \sum_{i=0}^{i=n} a_k a_i \cos \omega(t_k + t_i)$$

$$- \frac{1}{4} \sum_{k=0}^{k=n} \sum_{i=0}^{i=n} \sum_{j=0}^{j=n} \sum_{l=0}^{l=n} a_k a_i a_j a_l (\cos \omega(t_k - t_i + t_j - t_l)$$

$$+ \cos \omega(t_k - t_i - t_j + t_l))$$

$$- \sum_{k=0}^{k=n} \sum_{i=0}^{i=n} \sum_{j=0}^{j=n} a_k a_i a_j (\cos \omega(t_k + t_i - t_j)$$

$$+ \cos \omega(t_k - t_i + t_j)) + \dots$$

(3.6.4.5)

and hence we can deduce the power cepstrum from :

$$Y(\tau) = \int_{-\infty}^{+\infty} \{ \ln G_S(\omega) + 2 \sum_{k=0}^{k=n} a_k \cos \omega t_k$$

$$- \sum_{k=0}^{k=n} \sum_{i=0}^{i=n} a_k a_i \cos \omega(t_k + t_i)$$

$$- \sum_{k=0}^{k=n} \sum_{i=0}^{i=n} \sum_{j=0}^{j=n} a_k a_i a_j (\cos \omega(t_k + t_i - t_j)$$

$$+ \cos \omega(t_k - t_i + t_j))$$

$$\begin{aligned}
 & - \frac{1}{4} \sum_{k=0}^{k=n} \sum_{i=0}^{i=n} \sum_{j=0}^{j=n} \sum_{l=0}^{l=n} a_k a_i a_j a_l (\cos \omega(t_k - t_i + t_j - t_l) \\
 & + \cos \omega(t_k - t_i - t_j + t_l)) + \dots \} e^{-j\omega t} dt \quad (3.6.4.6)
 \end{aligned}$$

$$Y(\tau) = A\delta(t) + 2\pi \sum_{k=0}^{k=n} a_k (\delta(t+t_k) + \delta(t-t_k))$$

$$-\pi \sum_{k=0}^{k=n} \sum_{i=0}^{i=n} a_k a_i (\delta(t+t_k+t_i) + \delta(t-t_k-t_i))$$

$$-\pi \sum_{k=0}^{k=n} \sum_{i=0}^{i=n} \sum_{j=0}^{j=n} a_k a_i a_j (\delta(t+t_k+t_i-t_j)$$

$$+ \delta(t-t_k-t_i+t_j) + \delta(t+t_k-t_i+t_j) + \delta(t-t_k+t_i-t_j))$$

$$- \frac{\pi}{4} \sum_{k=0}^{k=n} \sum_{i=0}^{i=n} \sum_{j=0}^{j=n} \sum_{l=0}^{l=n} a_k a_i a_j a_l (\delta(t+t_k-t_i+t_j-t_l)$$

$$+ \delta(t-t_k+t_i-t_j+t_l) + \delta(t+t_k-t_i-t_j+t_l)$$

$$+ \delta(t-t_k+t_i+t_j-t_l) + \dots \quad \text{where } A \text{ is a constant.} \quad (3.6.4.7)$$

From this we can conclude that the number of delta functions quickly increases to infinity (for all practical purposes) for increasing m . ($m=0, 1, \dots, n$). This implies that for good multipath conditions (i.e. $m \approx 10$) we will not only have to identify the correct delta function corresponding to the different arrival times $t_0, t_1, t_2 \dots t_m$, but also the delta functions which exist with some symmetry axis about $t_0, t_1 \dots t_n$. This is clearly a difficult procedure. One could write a computer

program to test all the different delta functions for all possible symmetry axis starting with t_0 , but since so many symmetry axis exist this is felt to be quite a task, and beyond the scope for our investigation. In {3} it is stated that such a program for many arrivals would be almost impossible to construct. This is a view which this investigation completely shares.

3.6.5 The presence of noise

So far no noise considerations have been made. If we assume the simple case of additive noise $n(t)$ we have for the single echo case :

$$x(t) = s(t) + a_0 s(t-t_0) + n(t) \quad (3.6.5.1)$$

or

$$X(j\omega) = S(\omega) (1+a_0 e^{-j\omega t_0}) + N(\omega) \quad (3.6.5.2)$$

Since $S(\omega)$ and $N(\omega)$ usually are complex quantities we have :

$$|X(j\omega)| e^{j\theta_x} = |S(\omega)| e^{j\theta_s} (1+a_0 e^{-j\omega t_0}) + |N(\omega)| e^{j\theta_n} \quad (3.6.5.3)$$

Substituting $A = |S(\omega)|$ and $B = |N(\omega)|$ gives

$$\ln(|X(j\omega)| e^{j\theta_x}) = \ln(|A e^{j\theta_s} (1+a_0 e^{-j\omega t_0}) + B e^{j\theta_n}|) \quad (3.6.5.4)$$

After some manipulation this gives

$$\begin{aligned} \ln(|X(j\omega)| e^{j\theta_x}) &= \ln A + \frac{1}{2} \ln (1+a_o^2 + (\frac{B}{A})^2 \\ &+ 2a_o \cos(\omega t_o) + 2(\frac{B}{A}) \cos(\theta_s - \theta_n) \\ &+ 2a_o(\frac{B}{A}) \cos(\theta_s - \theta_n - \omega t_o)) \\ &+ j \tan^{-1} \left\{ \frac{\sin \theta_s + a_o \sin(\theta_s - \omega t_o) + (\frac{B}{A}) \sin \theta_s}{\cos \theta_s + a_o \cos(\theta_s - \omega t_o) + (\frac{B}{A}) \cos \theta_n} \right\} \end{aligned} \quad (3.6.5.5)$$

Now calculating the power cepstrum from the real part of (3.6.5.5) gives :

$$\begin{aligned} \text{Re}(\ln(|X(\omega)| e^{j\theta_x})) &= \ln A + \frac{1}{2} \ln((1+a_o^2 + (\frac{B}{A})^2 + 2a_o \cos(\omega t_o) \\ &+ 2(\frac{B}{A}) \cos(\theta_s - \theta_n) + 2a_o(\frac{B}{A}) \cos(\theta_s - \theta_n - \omega t_o)) \end{aligned} \quad (3.6.5.6)$$

Expanding (3.6.5.6) in terms of infinite series gives

$$\begin{aligned} \text{Re}(\ln(|X(\omega)| e^{j\theta_x})) &= \ln A + c + d \cos \omega t_o + e \cos(\theta_s - \theta_n) \\ &+ f \cos(\theta_s - \theta_n - \omega t_o) + g \cos(\theta_s - \theta_n + \omega t_o) \\ &+ h \cos(2\omega t_o) + i \cos(2(\theta_s - \theta_n)) \\ &+ j \cos(2(\theta_s - \theta_n - \omega t_o)) + k \cos(\theta_s - \theta_n - 2\omega t_o) \\ &+ l \cos(2\theta_s - 2\theta_n - \omega t_o) + \dots \end{aligned} \quad (3.6.5.7)$$

where

$$c = \frac{1}{4}(-a_o^4 - (\frac{B}{A})^4 - 4a_o^2 (B/A)^2)$$

$$d = a_o - a_o^3 - 2a_o (B/A)^2$$

$$e = (B/A) - 2a_o^2 (B/A) - (B/A)^3$$

$$f = -a_o^3 (\frac{B}{A}) - a_o (\frac{B}{A})^3$$

$$g = -a_o (B/A)$$

$$h = -\frac{1}{2} a_o^2$$

$$i = -\frac{1}{2} (B/A)^2$$

$$j = -\frac{1}{2} a_o^2 (\frac{B}{A})^2$$

$$k = -a_o^2 (B/A)$$

$$l = -a_o (B/A)^2$$

and hence we can deduce the power cepstrum from :

$$\begin{aligned}
 Y(\tau) = & \int_{-\infty}^{+\infty} (\ln A + c + d \cos \omega t_o + e \cos(\theta_s - \theta_n) \\
 & + f \cos(\theta_s - \theta_n - \omega t_o) + g \cos(\theta_s - \theta_n + \omega t_o) \\
 & + h \cos(2\omega t_o) + i \cos(2(\theta_s - \theta_n)) \\
 & + j \cos(2(\theta_s - \theta_n - \omega t_o)) + k \cos(\theta_s - \theta_n - 2\omega t_o) \\
 & + l \cos(2\theta_s - 2\theta_n - \omega t_o) + \dots) e^{-j\omega t} dt \quad (3.6.5.8)
 \end{aligned}$$

From this one can conclude that noise will affect both magnitude and phase.

When the magnitude of the noise is small with respect to the magnitude of the wavelet ($B \ll A$) and the amplitude of the echo (a_o) is less than unity, the real part of (3.6.5.5) reduces to the expression for the noise free case, as expected, that is

$$\text{Re} (\ln |X(\omega)| e^{j\theta_x}) = \ln A + a_o \cos \omega t_o - \frac{a_o^2}{2} \cos^2 \omega t_o + \dots$$

which should be compared with (3.6.2.12).

When the magnitude of the noise is not much less than that of the wavelet (again assuming $a_o < 1$) the other terms in (3.6.5.5) cannot be ignored, the resulting equation is rearranging (3.6.5.6) :

$$\begin{aligned} \text{Re}(\ln |X(\omega)| e^{j\theta_x}) &= \frac{1}{2} \ln(2AB \cos(\theta_s - \theta_n)) \\ &+ \frac{1}{2} \ln \left(1 + \left(\frac{B}{2A} + \frac{a_o^2 A}{2B} + \frac{A}{2B} \right) \frac{1}{\cos(\theta_s - \theta_n)} \right. \\ &+ \left. \frac{a_o A}{B} \cos \omega t_o \frac{1}{\cos(\theta_s - \theta_n)} + \frac{a_o \cos(\theta_s - \theta_n - \omega t_o)}{\cos(\theta_s - \theta_n)} \right) \end{aligned} \quad (3.6.5.9)$$

When the power cepstrum is computed from (3.6.5.9) (or (3.6.5.6)), particular attention must be given to the terms containing the quantities a_o and t_o since these parameters yield the desired echo information. If (3.6.5.9) is compared with (3.6.2.5) (noticing that the former is the real part of the log voltage spectrum while the latter is the log power spectrum), we see that the $\cos \omega t_o$ term in the absence of noise is multiplied by the term

$$\frac{1}{\cos(\theta_s - \theta_n)} \text{ when noise is present.}$$

From (3.6.5.8) it can further be concluded that we get delta functions at the desired epochs (t_o) plus the usual

multiple t_0 delta functions, but this time the multiple delta functions are modified with the noise angle. Thus making it impossible to sort out the true delta functions representing the epochs from the delta functions representing the different symmetry-axis - since generally the noise angle is not known.

3.6.6 Conclusion

The use of the cepstrum technique will give us delta functions at the different arrival times. In addition we will get delta functions at symmetry axis about the different epochs. These delta functions will be modified in the presence of noise. Our problem will then mainly consist of selecting and identifying the correct delta functions.

4 DATA COLLECTION

The area selected for the experiment is 15 nautical miles south of Arendal. This location has a fairly flat bottom profile with a water depth of 4 - 500 m.

Signals from a 7900 Hz source at a depth of 6.5 m were received and recorded. Figure 4.1 indicates the general geometrical principle. The receiver depth was approximately 60 m. Several recordings were made with distances between receiver and transmitter ranging from 1200 to 20 000 m. The pulse length was 60 mseconds.

Figure 4.2 is a block-diagram of the transmitting equipment. The power delivered to the transducer are 600 watt. The transducer efficiency is 60 %. Directivity (3 dB points) is 50° and 15° in the vertical respectively the horizontal plane.

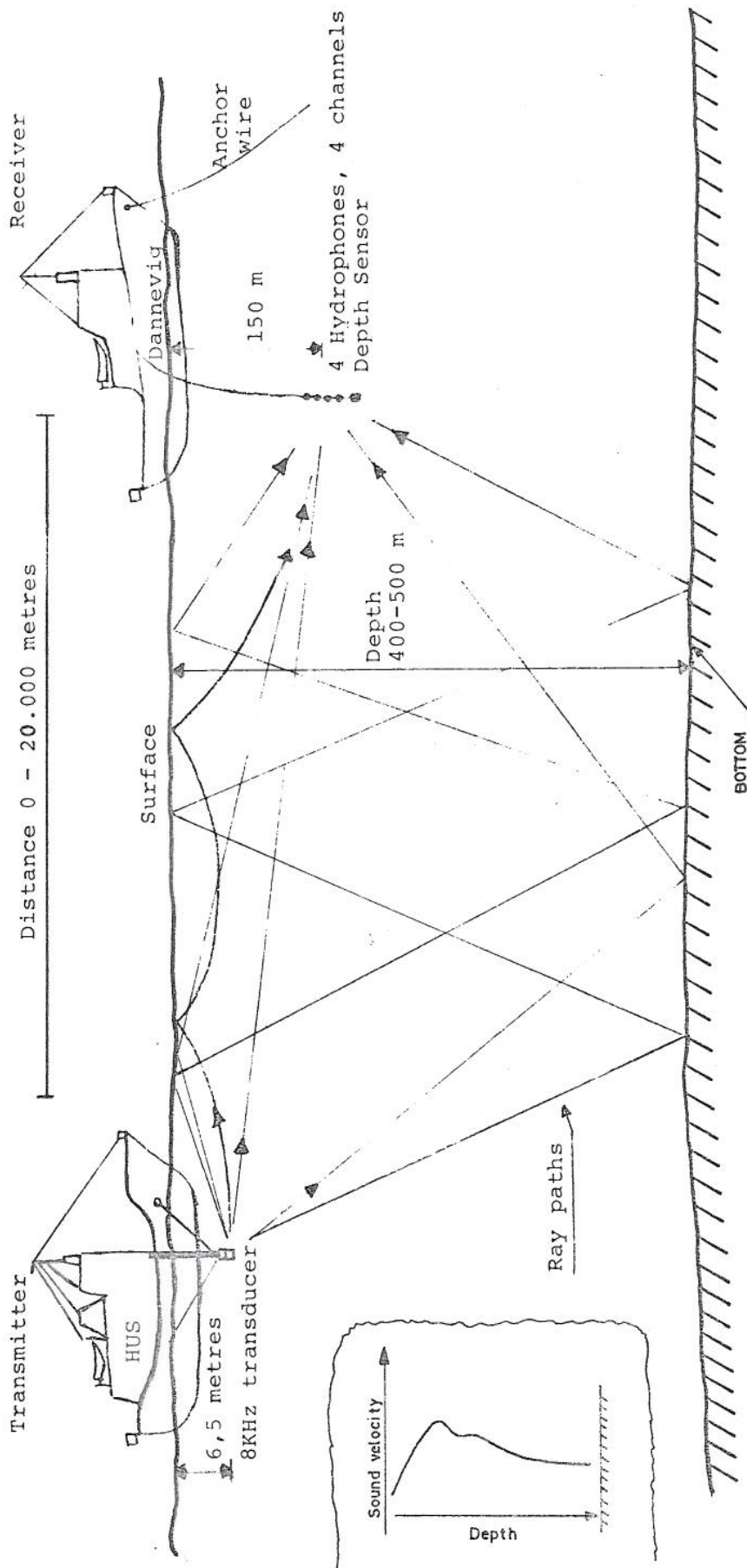


Figure 4.1 Measurement geometry

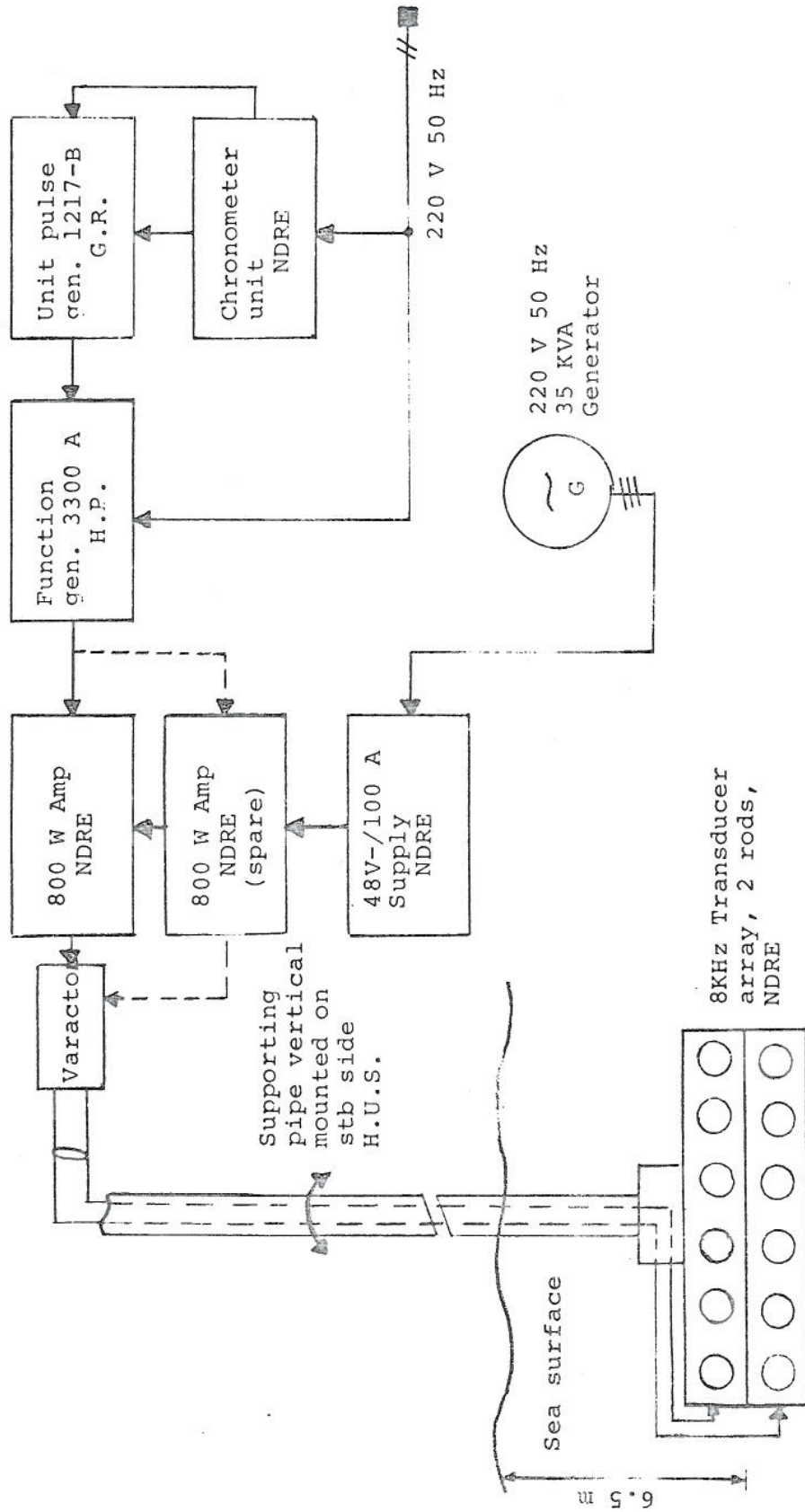


Figure 4.2 Transmitting equipment

Signal to noise ratio is about 20 dB at 10 000 m increasing to 48 dB at 1000 m. Silent ship conditions were established during the trials. Fig 4.3 is a block diagram of the receiving equipment and fig 4.4 indicates the recording system used.

Fig 4.5 shows the signal and noise structure and fig 4.6 gives a typical example of the signal received.

The hydrophone lobes indicated in fig 4.4 are formed by delay lines and a vertical array with four equally spaced hydrophones. We notice from fig 4.7 that the signal amplitude and phase depends on the lobe used.

A detailed description of the equipment and methods used during the trials can be found in {31}.

5 CALCULATION OF PROPAGATION PATHS

5.1 Sound velocity profiles

In section 2.1 and 2.2 some comments are given with reference to the propagation paths in shallow water. Fig 5.1 shows a typical sound velocity profile from research-cruise in March 1974. This type of velocity profile will lead to a surface channel effect. An assumption of isovelocity profile is clearly not valid and a computational method must be used which takes the sound velocity profile into account. Fig 5.2 shows a typical sound velocity profile from the research-cruise in November 1974. We can notice that the surface variation of sound velocity is quite different in the two cases shown. This will lead to different types of ray paths.

5.2 Calculations of ray paths

A method for calculating ray-paths has been developed at the NDRE. The procedure used is described in {26}. In {26} the ray theory for sound propagation in the sea is reviewed.

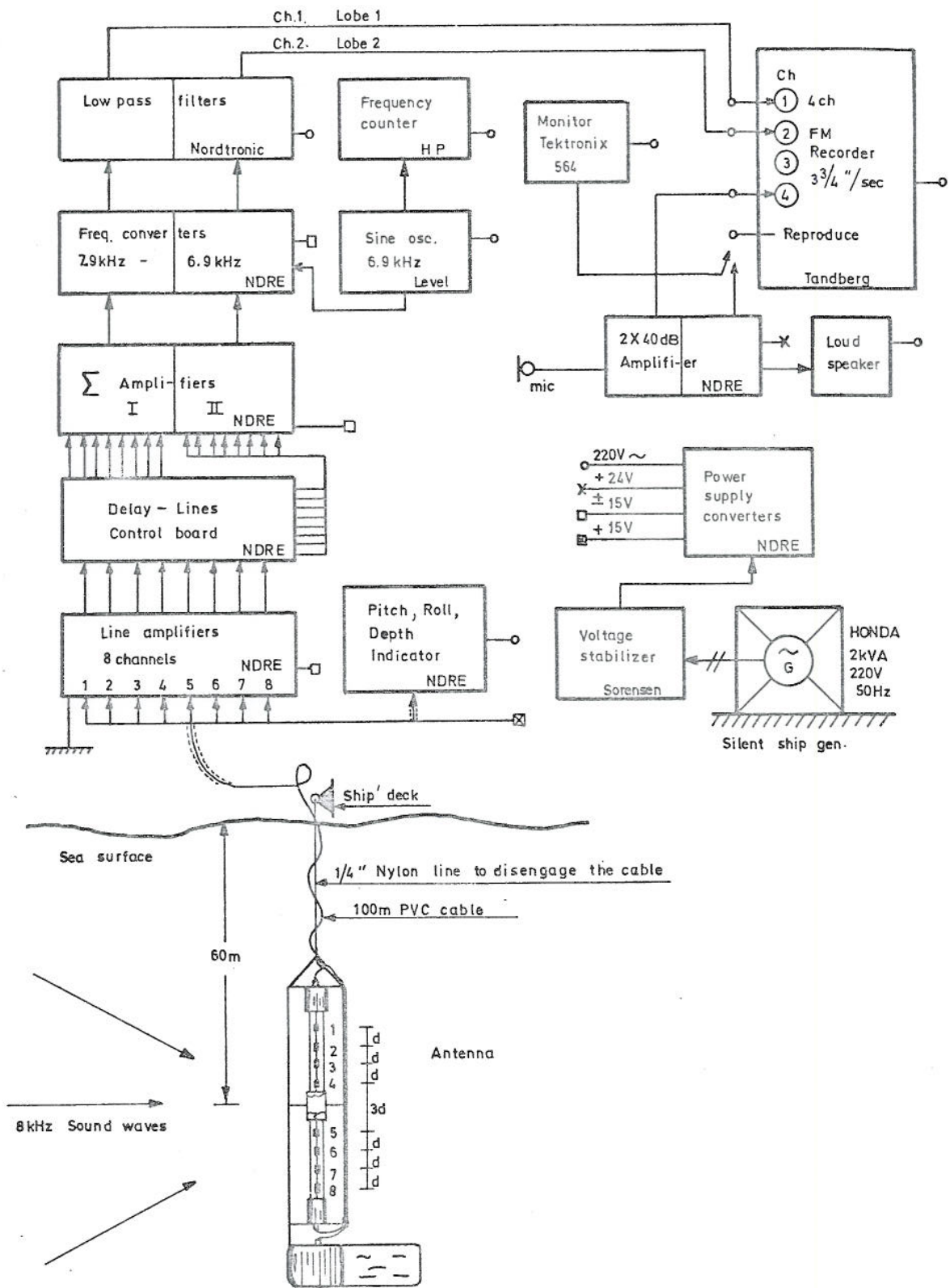


Figure 4.3 Receiving equipment

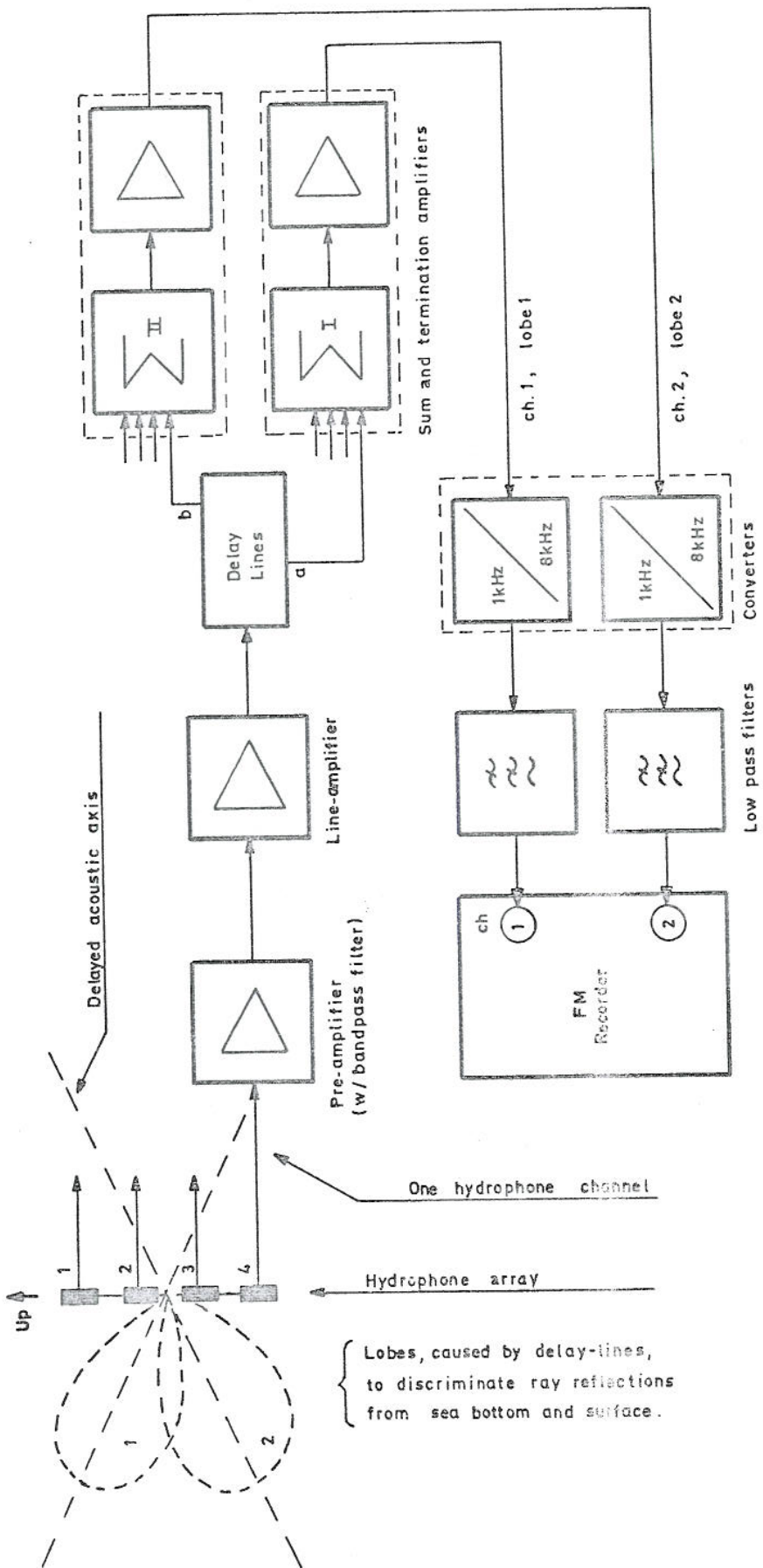


Figure 4.4 Signal recording system

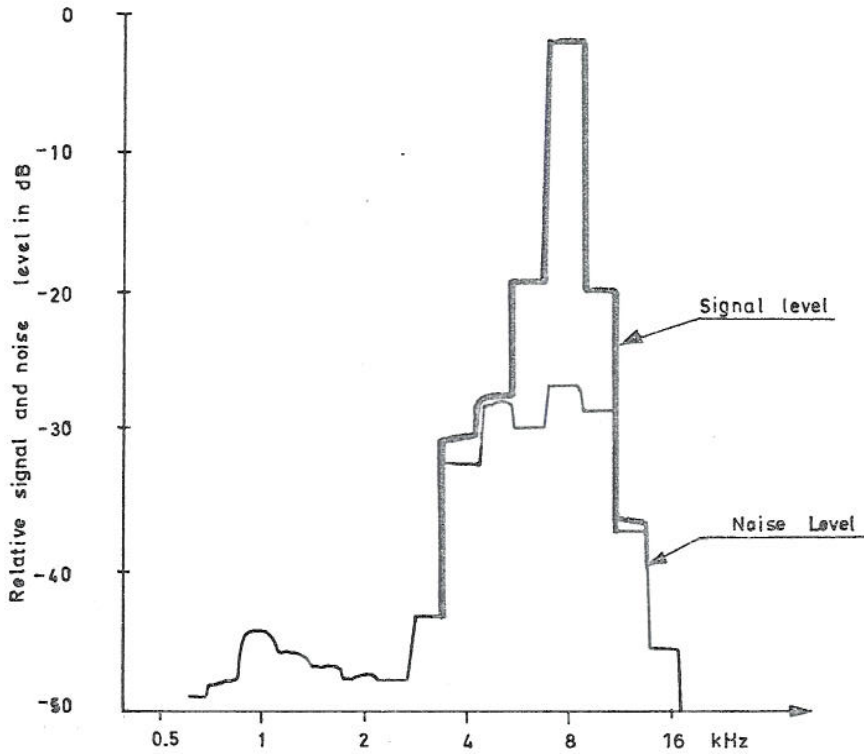


Figure 4.5 Signal and Noise versus frequency through 1/3 octave frequency analyzer, 1 msec pulse length, distance 4800m

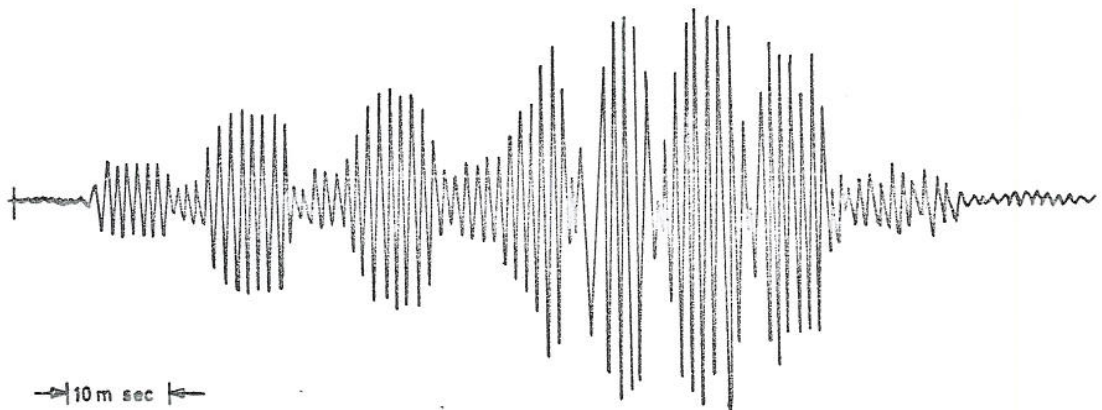


Figure 4.6 Typical signal structure, one hydrophone, 7.8 msec pulse length, frequency converted to 1 kHz, distance 5000m

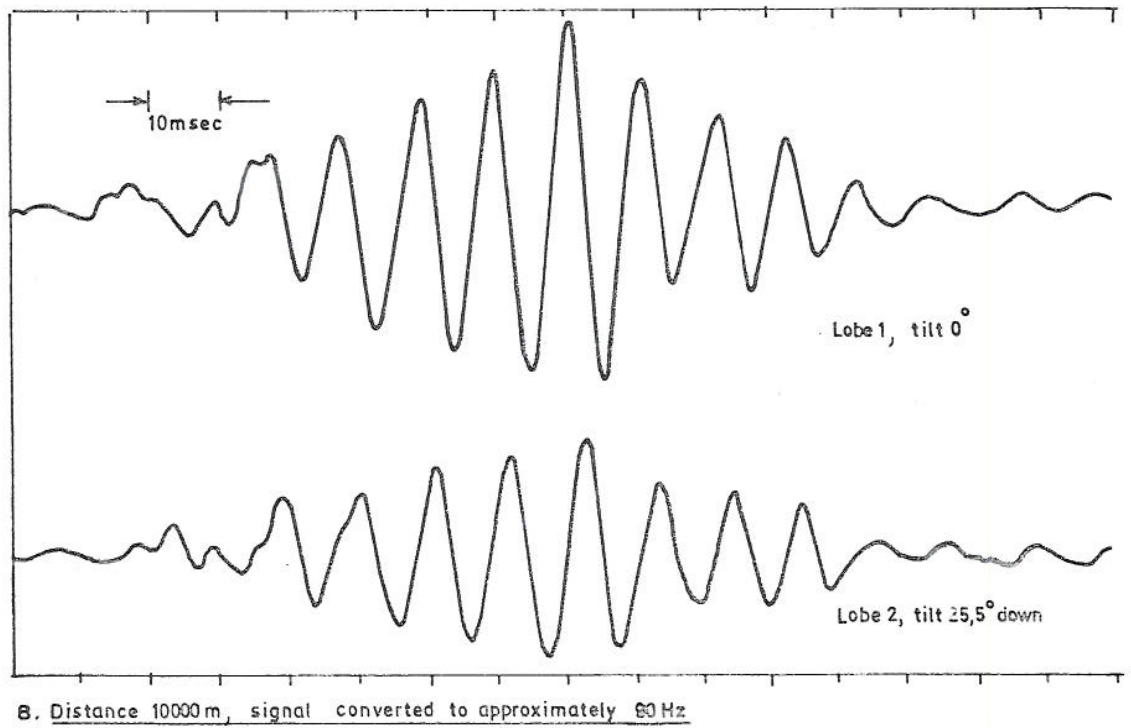
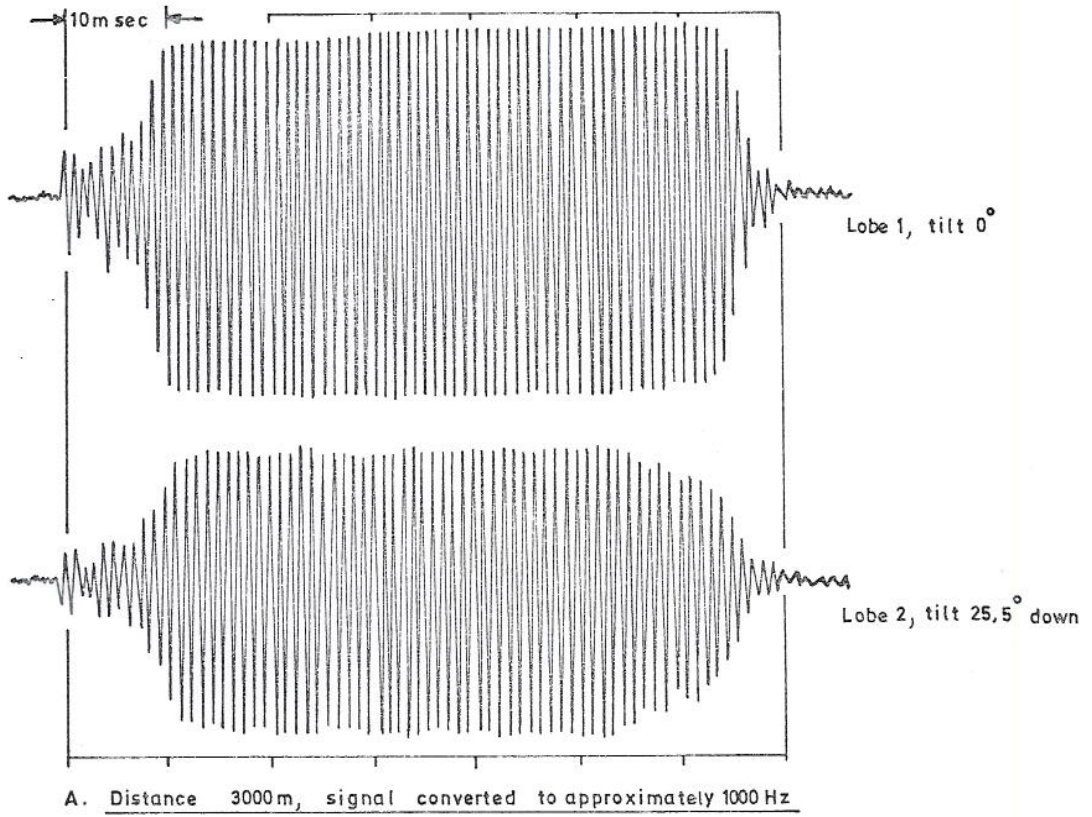


Figure 4.7 Signal structure examples, one array, two lobes.
Pulselength 60 msecs

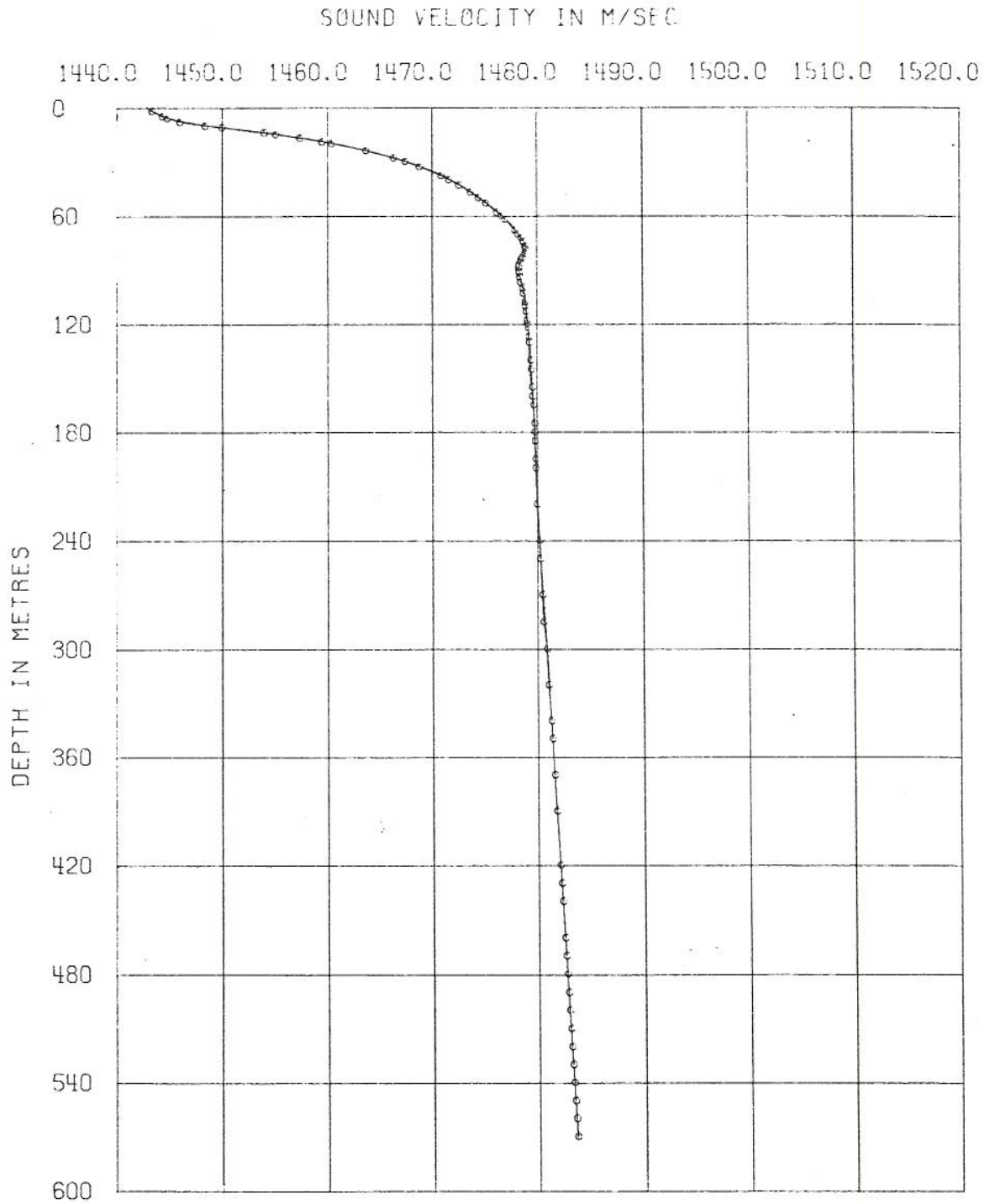


Figure 5.1 Sound velocity profile, March 1974

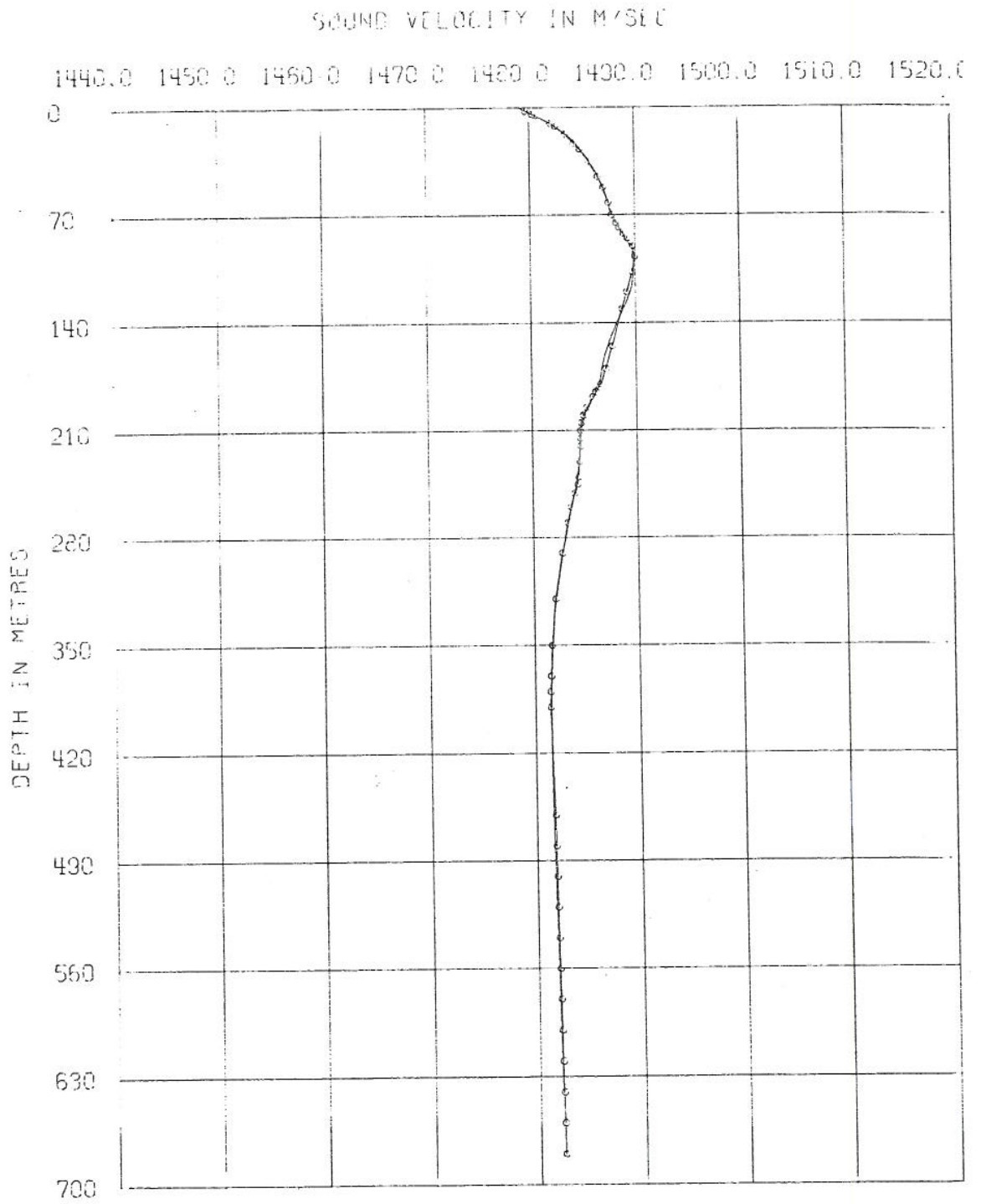


Figure 5.2 Sound velocity profile, November 1974

The theory is used in connection with an acoustic model of the ocean, the parameters of which are approximated by mathematical expressions. On this basis formulas for ray path coordinates, propagation time and intensity are developed. It should be stressed, however, that the computation is carried out on the following assumptions :

- (i) The ray theory must be valid, i e the depth of the sea must be at least ten times the wave length of sound. (In the present case the depth is approximately 450 m and the frequency used is 8 kHz thus obeying the stated requirement)
- (ii) The effect of reverberation is not taken into account
- (iii) The amount of energy which have propagated along the various ray paths are added at the end of the travel

Fig 5.3 shows the computed ray paths for a sound velocity profile of the type given in fig 5.1 and a bottom profile as indicated in fig 5.3. A strong channel effect can be noticed.

The transmission times obtained from the different transmission paths are tabulated and used for reference with the data obtained using the cepstrum technique (see section 6).

In fig 5.4 a flow-chart indicates the ray-tracing computation steps.

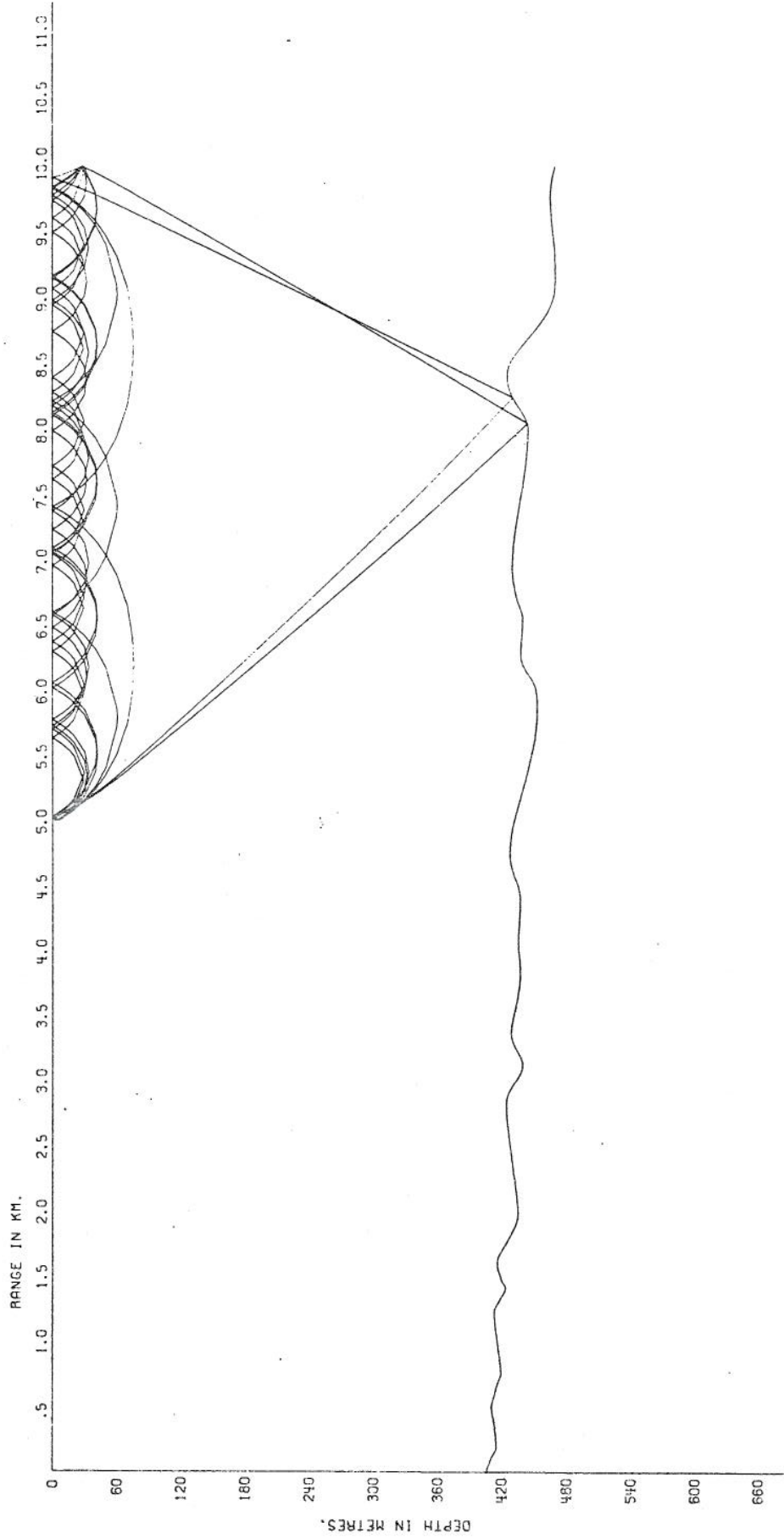


Figure 5.3 Possible ray paths with a bottom profile as indicated and the velocity distribution given in figure 5.1

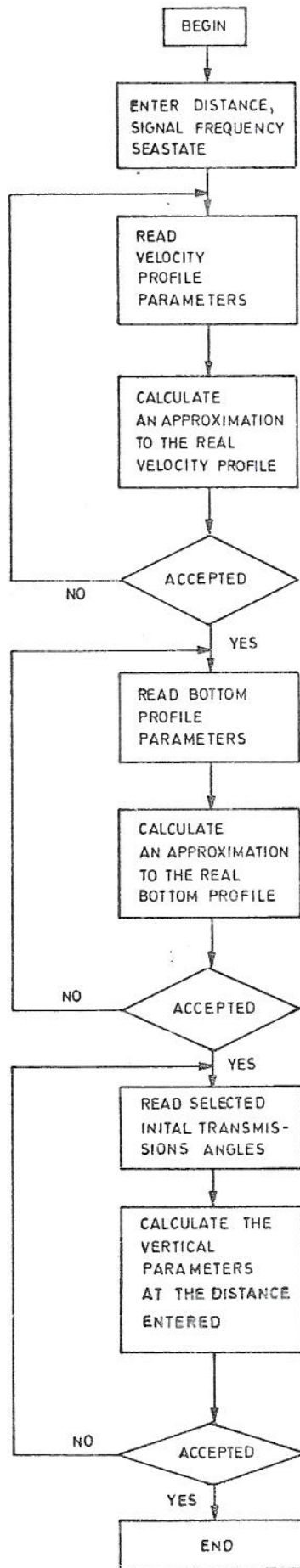


Figure 5.4 Flow-chart
Ray-Tracing Program

6 RESULTS

6.1 Implementation of the Cepstrum Method

The cepstrum method discussed above was implemented on a Nord-1 computer. A flow chart of the computer program is given in figure 6.1. There exist different types of implementations of the cepstrum method. The one chosen here is selected after trying out several of the in the literature suggested methods (see section 3.6). Our method differs slightly from the suggested ones since a second window function is used in order to reduce leakage after the second FFT. The use of the second window-function gives only marginally better results than without the window. There is no indication however that it gives poorer results, so the second window function is used throughout this analysis. The references {27} and {28} discuss the problems with leakage, aliasing etc in more detail. The computer program is written in FORTRAN IV and can be run on a computer with 32 k fast memory.

6.2 Results from simulated data

In order to test the computer program simulated data were used. Fig 6.2 shows a composite signal consisting of the original signal plus two echoes of identical shape, but smaller amplitudes (dotted lines). The method employed is seen to be very good with this simple signal. Different time delays between the signal and the echoes (i e different epochs) were used and echo resolution down to 2-3 parts pr 1000 units were possible. (For real data analysed below msec is the scale used). We notice the delta functions due to other symmetry axis as discussed above, but these are not dominant in this case.

A sinusoidal signal with two echoes is shown in figure 6.3. One may note that the echo resolution is very good and there can be no difficulties in identifying the two delta-functions due to the echoes. Also seen are delta functions due to several symmetry-axis. On either side of the delta function representing the start of the signal P_0 at time t , symmetry

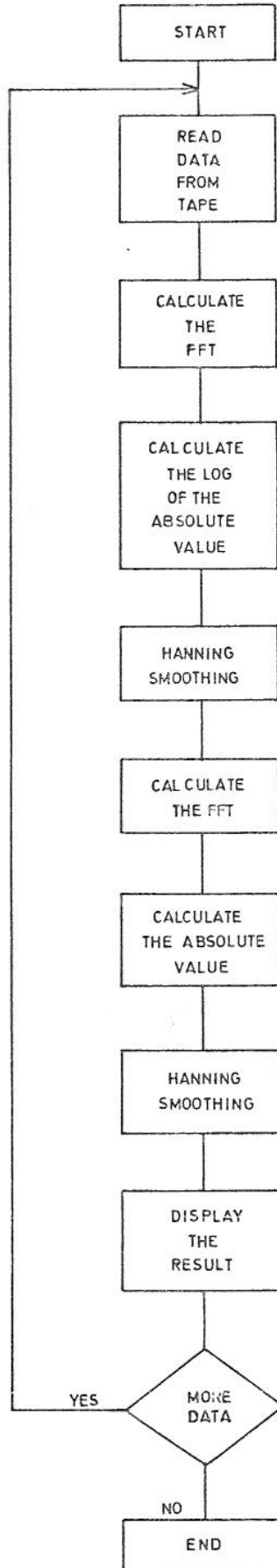


Figure 6.1 Flow chart - cepstrum program

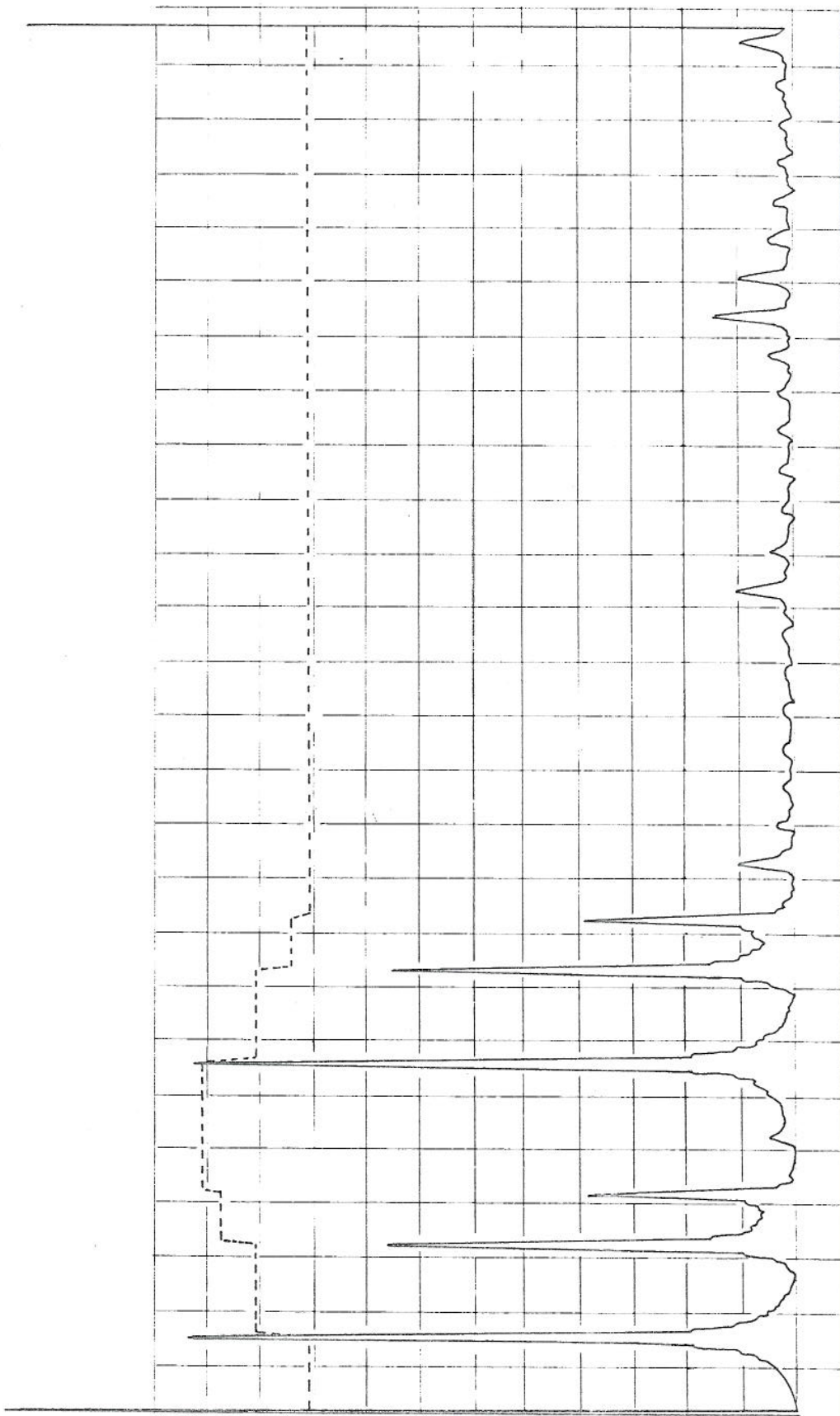


Figure 6.2 Cepstrum of a signal consisting of 2 echoes

CEPSTRUM

START 00
PING NO 00
DISTANCE 00

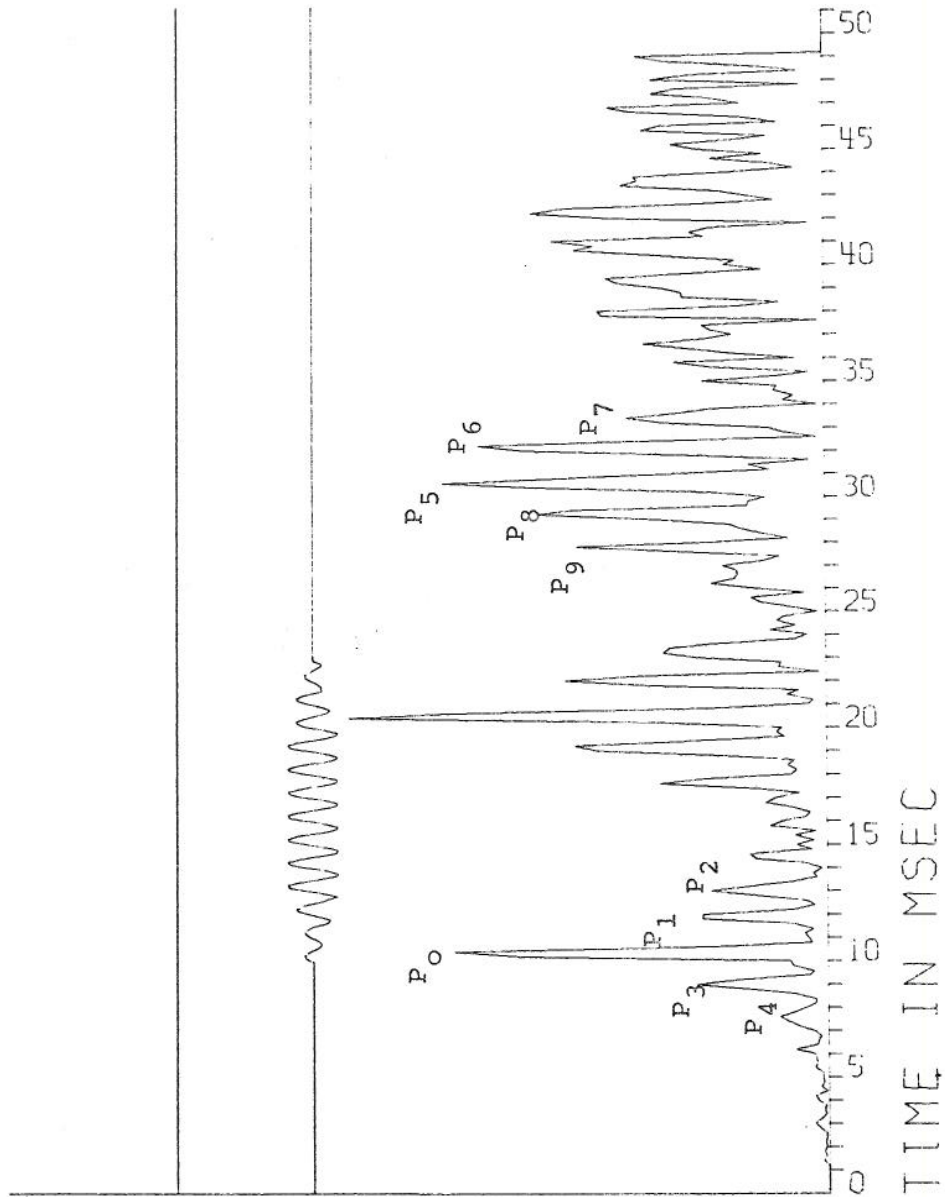


Figure 6.3 Cepstrum of a signal consisting of 2 echoes (at 10.0, 11.6, 12.8)
(For an explanation of the P's - see text)

can be seen. The peaks are P_1 at $t + \Delta t_1$ and P_2 at $t + \Delta t_2$ where Δt_1 is the time difference between the first arrival and the first echo, Δt_2 is the time difference between the first arrival and the second echo. We also have peaks at $t - \Delta t_1$ and $t - \Delta t_2$ (P_3 respectively P_4). Several other symmetry axis can also be easily identified. If we look at the $3t$ axis we have peaks at $3t$ (P_5), $3t + \Delta t_1$ (P_6), $3t + \Delta t_2$ (P_7), $3t - \Delta t_1$ (P_8), $3t - \Delta t_2$ (P_9).

The use of a simulated composite sinusoidal signal is of some interest since this is the same type of signal as used in our investigation. The computer model used is seen to give good results on simulated data. As noticed above most of the literature on related problems consist of investigation of simulated data. As is shown below these simulations may not always be in good agreement with real data.

6.3 Results from real data

Only the data from the research cruise in November were used. The data were converted to digital form at a sampling rate of 10 000 samples pr sec. (The Nyquist rate was roughly 4000). These data were read to the computer with record lengths of 10 000 samples and selected parts of this record were used for cepstrum calculations. Table 6.1 is obtained using the ray-tracing program described above. Only the position at 10240 m will be discussed in detail.

No of refl Bottom Surface		Time difference between echoes m secs	No of arrivals
0	2	0.0	1
1	1	25.0	2
1	0	26.2	3
1	2	32.1	4
1	1	35.6	5
2	1	92.5	6
2	2	94.1	7
2	2	105.4	8
2	3	107.0	9

Table 6.1 Calculated Echo arrival times at 10 240 m

One can note from figures 6.5, 6.6 and 6.7 :

- (a) The received signal varies greatly from ping to ping
- (b) The cepstrum method fails to give a clear identification of the echoes if only one cepstrum at the time is considered
- (c) The cepstrum method does give a delta function (or rather a peak) at the correct value. However, it is difficult to pick the correct peaks from the ones due to symmetry and/or due to noise.

As noted the received signal varies greatly from ping to ping. This can be regarded as a form of noise. Due to variations in the transmission media which vary in a stochastic way it is difficult (or often impossible) to predict this "impedance" variation. Figures 6.5, 6.6 and 6.7 shows that the SNR of the signals are good, and background noise due to the sea is negligible. It is reasonable to assume that this stochastic variation in the "impedance" of the transmission media will vary with time and space. Thus the stationarity of the transmission media can be questioned. Normally we will assume stationary conditions when the time span of the observations are short. This quasi-stationary condition is assumed in this report. Furthermore, signal degradation due to reflections at the sea-bottom or the surface will add to the stochastic variation.

We are therefore forced to work on echoes which are not replicas of the first arrival, and there is very little we can do to improve this situation.

The most prominent peaks (4-5) in each cepstrum were noted and plotted in the histogram given in figure 6.8. The calculated arrival times are indicated with arrows. From this one can conclude :

CEPSTRUM

START 4100
PING NO 102
DISTANCE 10241

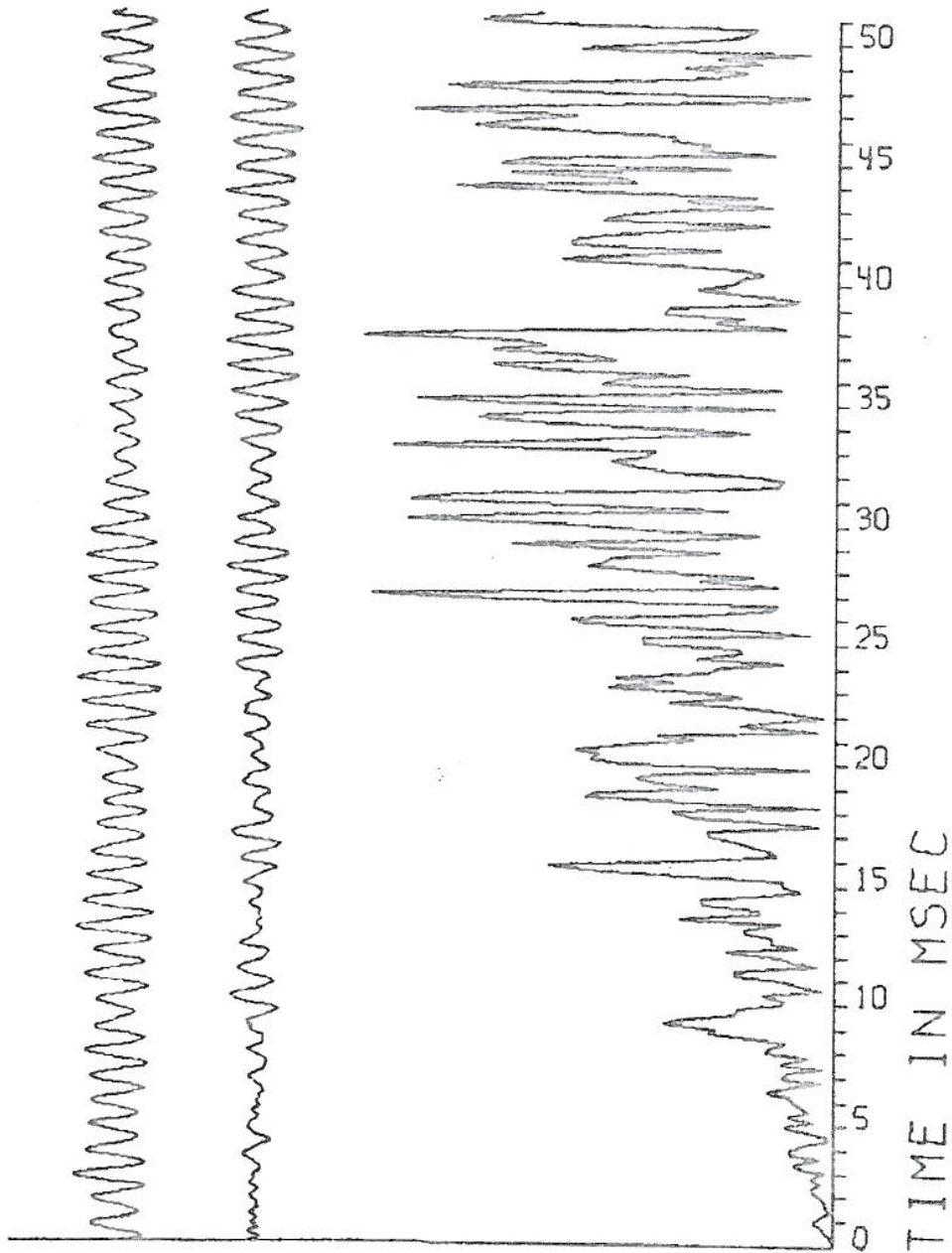


Figure 6.4 A 60 msec pulse received at a distance of 10240 m with corresponding cepstrum. (The received pulse start at lower left and continuous from lower right t_0 upper left t_0 upper right)

CEPSTRUM

START 8400
PING NO 104
DISTANCE 10241

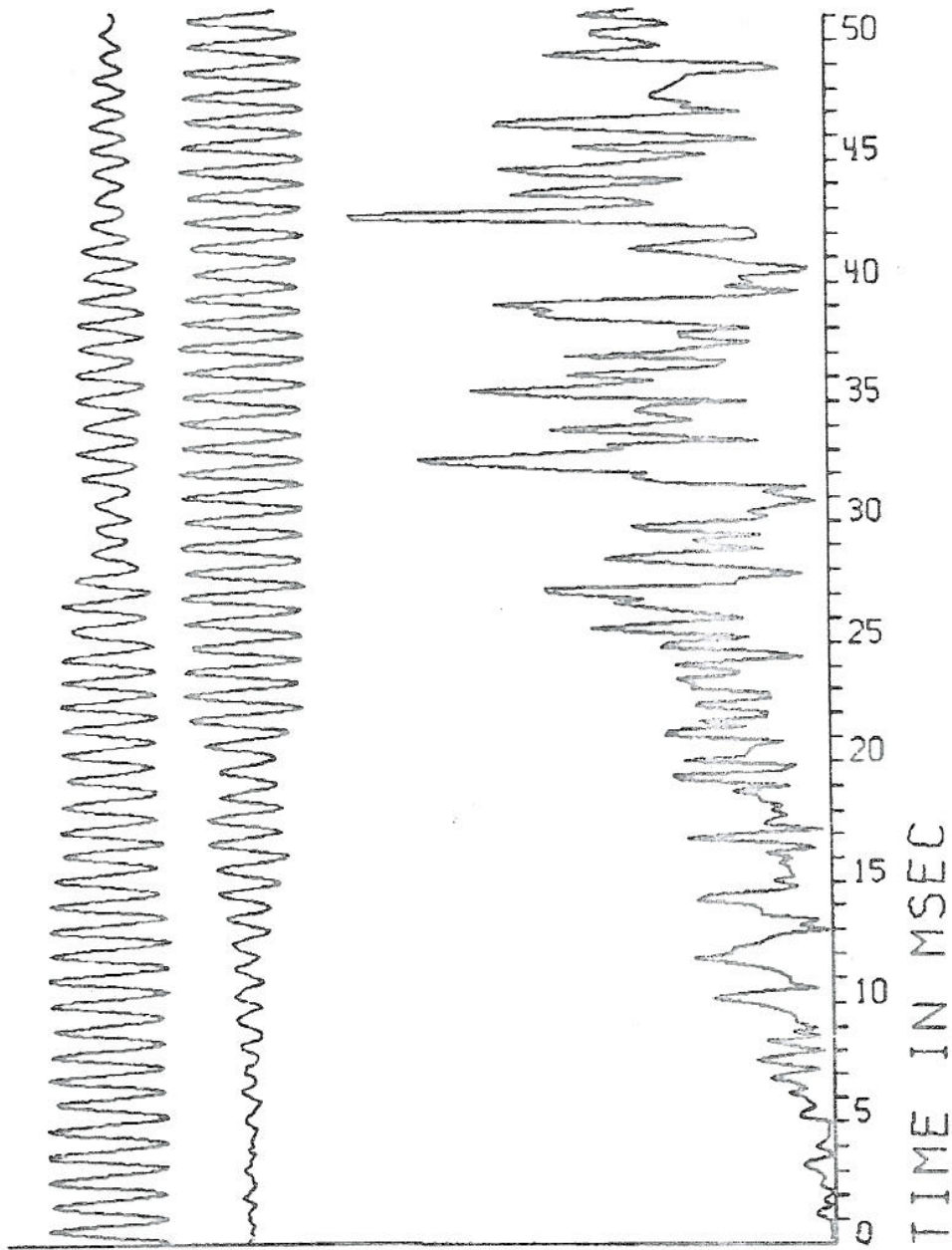


Figure 6.5 A 60 msec pulse received at a distance of 10 240 m with corresponding cepstrum. (The received pulse start at lower left and continuous from lower right t_o upper left t_o upper right)

CEPSTRUM

START 1150
PING NO 108
DISTANCE 10241

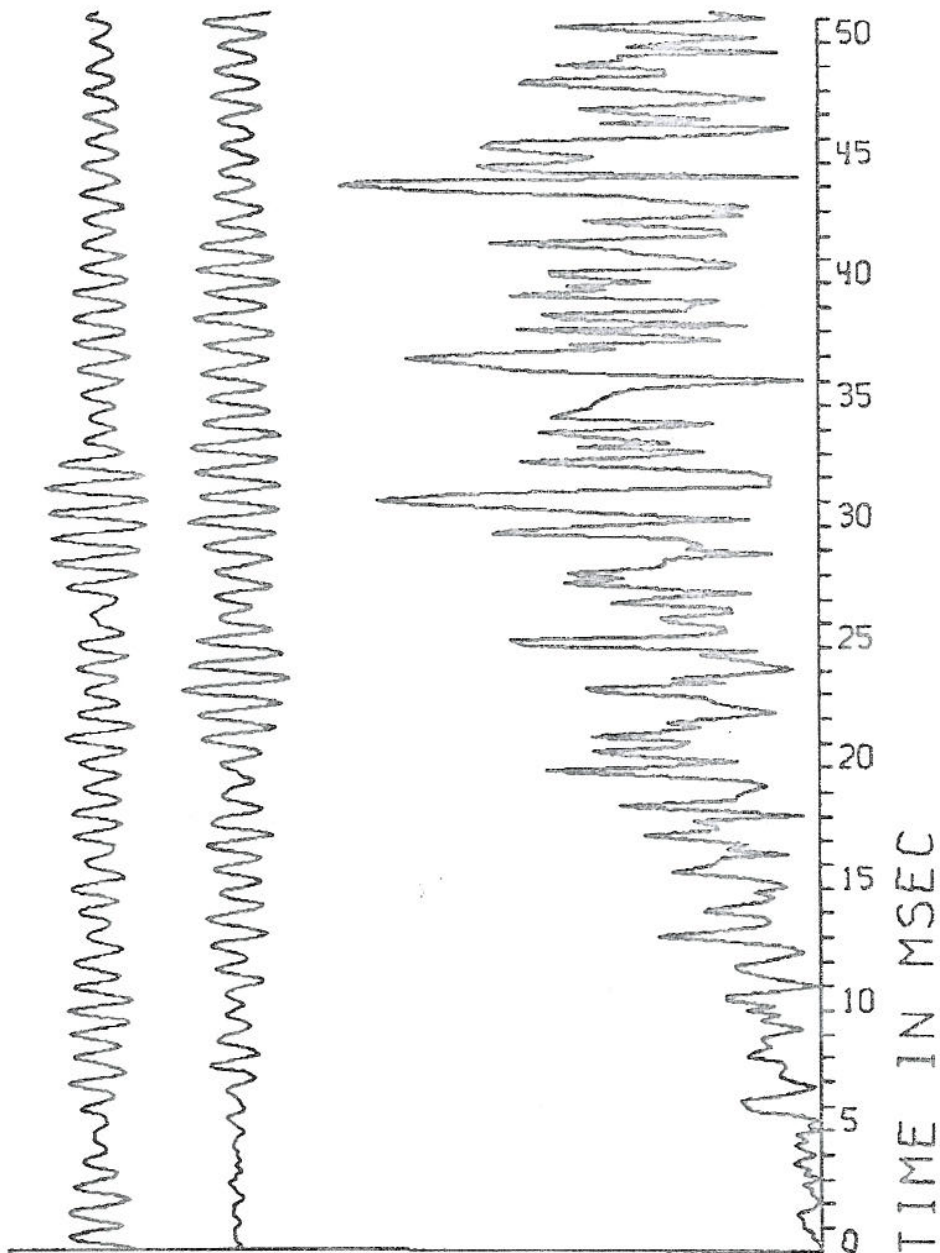
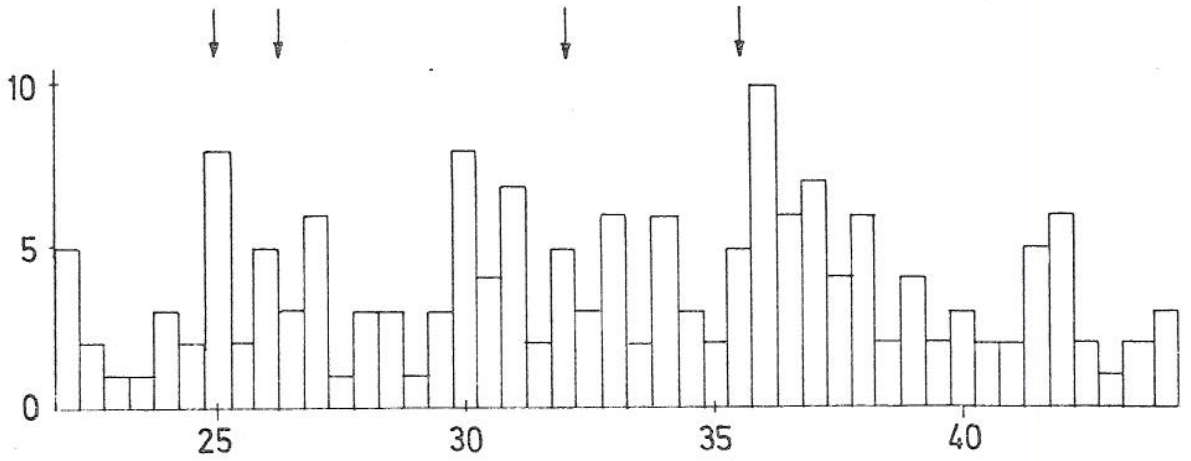
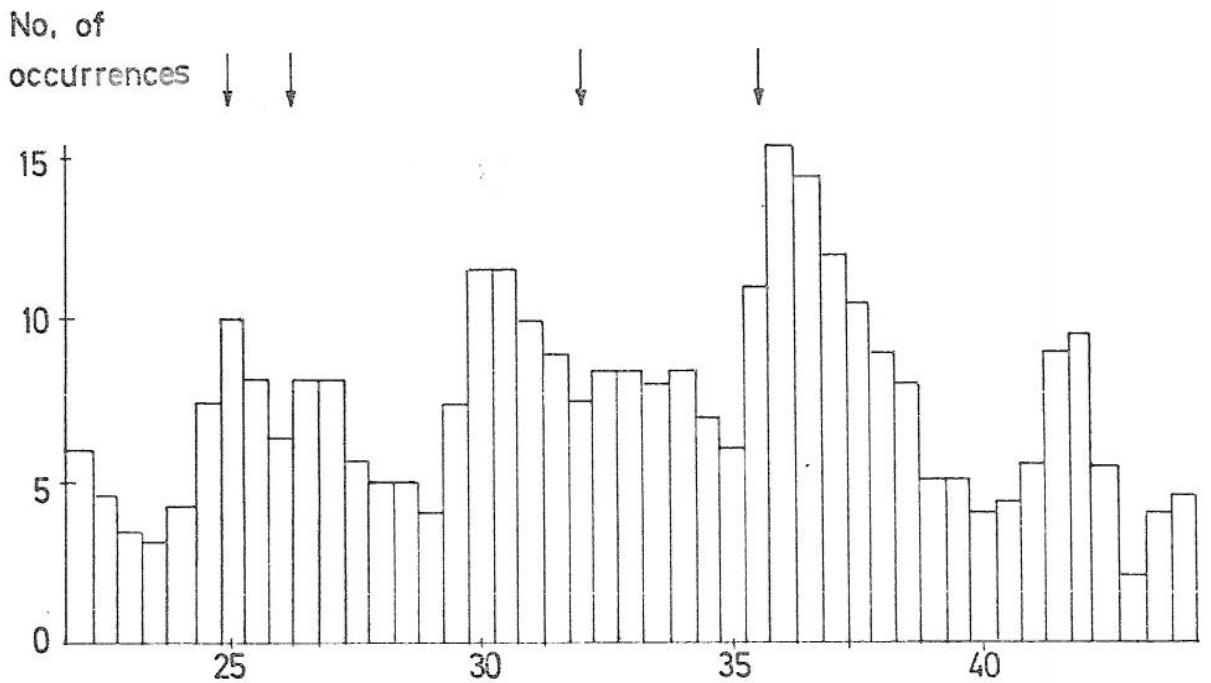


Figure 6.6 A 60 msec pulse received at a distance of 10 240 m with corresponding cepstrum. (The received pulse start at lower left and continuous from lower right to upper left to upper right)



Original data for n = 35. Arrows indicate expected arrival times



Smoothed data for n = 35, arrows indicate expected arrival times

Figure 6.7 Histograms of the no of occurrences of dominant cepstrum peaks (n=35)

- (d) A consistent pattern of dominant peaks occurs at or near the calculated arrival times
- (e) two extra peaks occurs. There may be several reasons for these extra peaks
 - (i) due to symmetry
 - (ii) due to truncation of the signal
 - (iii) due to noise (i e background noise, stochastic variations in the transmission media and degradation due to reflections)
- (f) By using two different sets of data
 - one with a beam pattern tilt of 12.75° and one with 0° - no difference in the cepstrum information was possible to notice

An analysis similar to the one above was conducted on the data from 3000 m. In this case a peak at 1 msec is expected. However, it was not possible to obtain this. The reason for this failure is probably because we use a cosine window - function in our cepstrum program which will reduce the peak of the earlier arrival times. Thus the program implemented here is not suited for arrival time differences shorter than 5 msec and longer than 45 msec. By rewriting the program slightly and deemphasizing the window-function effect by multiplying with the inverse window-function a cepstrum with the greatest emphasis on the first 10-15 msec were obtained. This method gave a clear identification of the wanted arrival time, but it is felt that this result would not have been obtained if we had not a priori known the "correct" result.

6.4 Comparison with results obtained using correlation technique

In {30} the correlation technique is used in determining differences in arrival times between paths of a transmission channel. With undistorted and time delayed signals in Gaussian noise, the cepstrum technique behaves close to a

maximum likelihood estimator, thus surpassing the performance of the autocorrelation technique {18}. As noted in section 6.3 this is not a realistic situation since variations in the transmission channel due to other effects are dominating.

It is shown in {30} that the auto-correlation processing would outperform cepstrum processing when the distortion effects dominate in the transmission channel. Auto-correlation does not, however, work well with strong sinusoidal components in the signal. A filtering method to remove the component due to the sinusoids in the power spectrum must be used.

7 CONCLUSIONS

The use of the cepstrum method will give an indication of the epochs when several cepstrums are considered for dominant peaks. It is felt that due to the fluctuations of the signals the assumption made in our mathematical analysis that the echoes are identical in shape to the first arrival is not correct. However, the results obtained are under these circumstances acceptable. The cepstrum technique will not give perfect results due to signal fluctuations. It is difficult to see that other methods can be substantially better since signal fluctuation will occur, thus one is dealing with imperfect replicas of the original signal. Noise of random type, will not affect the cepstrum method to such an extent as fluctuations due to changes in transmission media, bottom reflections and surface scattering.

From Table 6.1 one can notice that the direct signal ($B = 0, S = 0$) and one of the echoes due to one reflection ($B = 0, S = 1$) are missing. In shallow water and at great distances (10 000) this is probably a normal situation. A situation with these missing rays present might give better (or more closely identifiable) peaks.

REFERENCES

- (1) Riter et al Pulse Position Modulation Acoustic
communications
IEEE vol AU-19 No 2, pp 166-173, June 1971
- (2) Senmoto and Adaptive Decomposition of a Composite
Childers Signal of Identical Unknown Wavelets
in Noise
IEEE vol SMC-2 pp 59-66 Jan 1972
- (3) Kemerait and Signal Detection and Extraction by
Childers Cepstrum Techniques
IEEE vol IT-18, No 6, pp 745-759, Nov 1972
- (4) Childers et al Composite signal decomposition
IEEE vol AU-18 pp 471-477 Dec 1970
- (5) Senmoto and Signal resolution via digital inverse
Childers filtering
IEEE vol AES-8, No 5, pp 663-640, Sept
1972
- (6) Barton Comments on Signal resolution via digital
inverse filtering
IEEE vol AES-9, No 4 pp 607-608, July 1973
- (7) Paul and Remarks on Comments on Signal Resolution
Nunn via digital inverse filtering
IEEE vol AES, No 2 pp 293-295, March 1974
- (8) Barton Further comments on inverse filtering
IEEE vol AES-10, No 2, pp 294-295
March 1974
- (9) Markel Digital inverse filtering - a new tool
for formant trajectory estimation.
IEEE vol AU-20, No 2, pp 129-137, June -72
- (10) Moore and On nonlinear filters involving trans-
Parker formation of the time variable
IEEE vol IT-19, No 4 pp 415-422 July 1973
- (11) Oppenheim et al Nonlinear filtering of multiplied and con-
volved signals
Proc IEEE vol 56, No 8, pp 1264-1291,
Aug 1968
- (12) Bucy Linear and nonlinear filtering
Proc IEEE vol 58, No 8 pp 854-864,
June 1970

- (13) Fisher and Stear Optimal nonlinear filtering for independent increment processes Part I vol IT - 3, no 4 pp 558-568, Oct 1967
- (14) Fisher and Stear Optimal nonlinear filtering for independent increment processes Part II vol IT-3, no 4 pp 568-578, Oct 1967
- (15) Chua Synthesis of new nonlinear network elements Proc IEEE vol 56 no 8 pp 1325-1340, Aug 1968
- (16) Hassab On the convergence interval of the power cepstrum IEEE vol IT, pp 111-112, Jan 1974
- (17) Bøhme The cepstrum as a generalized function IEEE vol IT, pp 650-653 Sept 1974
- (18) Bogert and Ossana The heuristics of Cepstrum Analysis of a stationary complex echoed gaussian signal in stationary gaussian noise IEEE vol IT-12, no 3 pp 373-380, July 1966
- (19) Bogert et al The frequency analysis of time series for echoes : cepstrum, pseudoautocovariance, cross-cepstrum and saphe-cracking in Time Series Analysis M Rosenblatt Ed New York : Wiley 1963 ch 15
- (20) Noll Short time spectrum and cepstrum techniques for vocal-pitch detection JASA vol 36 pp 296-302 Febr 1964
- (21) Schafer and Rabiner System for automatic formant analysis of voiced speech JASA vol 47 no 2 part 2 pp 634-648 1970
- (22) Oppenheim and Schafer Homomorphic analysis of speech IEEE vol AU-16, pp 221-226 Jan 1968
- (23) Oppenheim Speech analysis - synthesis system based on homomorphic filtering JASA 45, pp 458-465, 1969
- (24) Noll Cepstrum pitch determination JASA vol 41 no 2 pp 293-309, 1967
- (25) Meek A note on the mathematics of the cepstrum and on alternate Univ Texas, Austin, Defence Res Lab Techn memo 68-32 (DRL-TM-68-32) Dec 6, 1968

- (26) Aubell Theoretical calculation of intensities
and transmission loss in the ocean
NDRE IR.U-261 Dec 1970
- (27) Bergland A guided tour of the fast Fourier trans-
form
IEEE Spectrum July 1969
- (28) Ramirez The fast Fourier transform's errors are
predictable, therefore manageable
Electronics June 13, 1974
- (29) Hassab On the multipath problem
NUSC, Working Memorandum No 67-72 (conf)
- (30) Hassab The delay processing near the ocean
surface
J Sound and Vibration (1974)
35(4), 489-501
- (31) Dammen NDRE TN 1975 (In preparation)